



MSc Thesis

---

# **Study on the influence of air leakage in working face on gas flow field in goaf of Y-type ventilation system**

---

**Haohui Shi**

06/05/2019

---

School of Emergency Management and Safety Engineering  
China university of mining and technology  
Beijing, Haidian district, Xueyuan road, ding 11  
Zonghe Building 246  
Phone: +86 13263129266  
ehsshihaohui@163.com



---

## **Declaration of Authorship**

---

„I declare in lieu of oath that this thesis is entirely my own work except where otherwise indicated. The presence of quoted or paraphrased material has been clearly signaled and all sources have been referred. The thesis has not been submitted for a degree at any other institution and has not been published yet.”



---

## Abstract

---

This paper takes the W1310 fully mechanized caving face of Wuyang Coal Mine of Lu'an Mining Bureau as the research object. First of all, I studied several different ventilation methods of coal mines, as well as the advantages and disadvantages of Y-type ventilation systems. The research status of scholars in various fields in the Y-type ventilation system and high-drainage alleys is explored.

Through theoretical analysis, numerical simulation and application of numerical simulation software, the internal roof of the coal mine goaf and the rock permeability are promoted with the advancement of mining operations, and the regularity of the roof of the goaf is changed. The distribution of “three district” and “three zones” in coal mines was studied, which provided data support for further numerical simulation of goafs. After the basic information of the goaf is set, the internal flow field of the goaf is simulated with the change of the ventilation system, and the migration law and concentration distribution of the gas in the goaf are further simulated. Finally, the influence of high pumping lanes was added to the simulation, and a simulation example of the gas distribution law of the W1310 goaf in Gaohe Coal Mine was obtained.

At the same time, I also obtained a series of downhole measurements to obtain the gas concentration distribution at different locations in the working face. It is proved that the gas in the working face is different from the gas distribution from the inlet to the return air. At the same time, the SF<sub>6</sub> wind leakage instrument was also used to investigate the air leakage in the goaf and the roadway along the goaf, and the simulation results were verified.

Keyword:

Y-type ventilation; high extraction roadway; SF<sub>6</sub>; air leakage; gob-side entry retaining.

---

# Table of Contents

---

Declaration of Authorship.....	II
Abstract.....	IV
Table of Contents.....	V
1 Introduction.....	1
1.1 Research Background and Significance.....	1
1.2 Research Status.....	2
1.2.1 Research Status of Y-type Ventilation.....	2
1.2.2 Study on the law of gas migration in goaf.....	3
1.2.3 Gob area gas drainage technology.....	3
1.3 Project research content and method.....	4
1.3.1 research content.....	4
1.3.2 Research methods.....	5
1.4 chapter summary.....	6
2 Theoretical Analysis of Gas Migration and Fracture Evolution in Goaf.....	7
2.1 Porous medium model.....	7
2.2 Mathematical Model of Gas Migration in Goaf.....	8
2.2.1 Continuity Equation.....	8
2.2.2 momentum conservation equation.....	9
2.2.3 Component transport equation.....	10
2.3 Summary of this chapter.....	13
3 Study on Numerical Simulation of gas migration in goaf of mining fissures and Y-type ventilation system.....	15
3.1 Overview of working face.....	15
3.2 Standard goaf seepage model.....	15
3.2.1 Empirical Model of Void and Permeability.....	16
3.2.2 Three-dimensional permeability model.....	18
3.3 Numerical simulation of mining fissure evolution.....	19
3.3.1 Introduction to UDEC Numerical Simulation Software.....	19
3.3.2 Establishment of UDEC numerical model.....	20
3.4 Summary of chapter.....	23
4 Study on Numerical Simulation of gas migration in goaf of Y-type ventilation system.....	25
4.1.1 Introduction to COMSOL Software.....	25

4.1.2	Establishment of COMSOL physical model.....	25
4.1.3	Boundary Conditions Setting.....	26
4.2	simulation results analysis.....	26
4.2.1	Vertical Direction of Goaf.....	27
4.2.2	Direction of Vertical Working Face.....	28
4.2.3	Numerical simulation results under high pumping conditions.....	29
4.3	Summary of this chapter.....	31
5	Analysis and Measurement of Air Leakage Law of Fully Mechanized Caving Face.....	33
5.1	Y-type working face pressure energy analysis.....	33
5.1.1	Barometer method.....	33
5.1.2	Analysis of Pressure Energy Distribution in Working Face.....	34
5.2	Work surface leakage measurement.....	37
5.2.1	Tracer gas method for measuring the principle of air leakage.....	37
5.2.2	SF6 gas release and detection device.....	38
5.2.3	Estimation of Tracer Gas Release.....	40
5.2.4	Measuring Point Arrangement Scheme.....	41
5.2.5	data processing.....	43
5.2.6	Result and Analysis.....	48
5.3	Summary of this chapter.....	50
6	Conclusion.....	51
6.1	Main conclusions.....	51
6.2	Outlook.....	52
6.3	Innovation points.....	52
7	Bibliography.....	53
8	List of Figures.....	57
9	List of Tables.....	59





---

# 1 Introduction

---

In this paper, the main numerical simulation and on-site measurement methods are used to study the gas migration law in coal mine goaf.

---

## 1.1 Research Background and Significance

---

In the past ten years, China's coal mining technology has developed rapidly. But the coal mining face is longer, and the disturbance of coal mining to coal and rock mass is larger. The result is that the gas flowing into the working face in the goaf rises, which poses a threat to the safe production of the mine [1]. Research shows that coal mine gas mainly comes from goaf of coal mine working face. The original ventilation method is increasingly unable to meet the needs of safe production. Traditional ventilation modes include U-type ventilation, W-type ventilation and U + L ventilation. Compared with the Y-type ventilation method, part of the gas in the common ventilation mode accumulates on the working surface, causing the gas to exceed the limit. In order to solve the problem of excessive gas in the working face and the upper corner, Y-type ventilation is used to leak air into the return air passage, and the gas in the goaf is forced into the return air passage [2]. The function of the auxiliary air inlet channel is to disperse the gas concentrated in the upper corner and dilute the gas concentration in the return air passage to a safe and reasonable numerical range.

**Table 1 Flow field and gas concentration distribution in goaf under different ventilation modes**

Ventilation method	Wind flow field	Gas concentration distribution
U-type ventilation	In addition to flowing along the working surface, a part of the wind flows into the goaf and emerges from the working surface half [3].	The gas concentration in the goaf and return airway is high [2].
W-type ventilation	Part of the wind flows along the work surface, and another part enters the the goaf, and the wind converges from the middle of the work surface.	The gas concentration in the goaf is centered on the middle of the work increases along the goaf [4].

---

---

U+L-type ventilation	<p>A large amount of gas in the pressure relief zone is directed to the inner tailgate, and the extraction effect causes the high concentration gas in the goaf to move to the suction port [5].</p>	<p>The gas concentration in the goaf, return airway and upper corner is reduced, and the gas concentration in the tailgate is increased.</p>
Y-type ventilation	<p>Part of the wind flows along the working surface, and the other part flows into the gob along the streamline, and finally flows out along the empty roadway [2].</p>	<p>The concentration of gas near and in the goaf is higher [6, 7].</p>

---



---

## 1.2 Research Status

---

### 1.2.1 Research Status of Y-type Ventilation

---

In China, the Y-type ventilation of coal mines is an excellent way to deal with mine gas problems [11]. Whether it is Huaibei or Yangquan. At the same time, because of the increasing use of Y-type ventilation, major coal mines and universities have begun to study more mechanisms.

Wang Shengshen and Cheng Yuanping passed the actual measurement and simulation. They studied the ventilation system and gas distribution law of major coal mines in China. The changes of wind flow and gas migration under different ventilation modes are analyzed [12]. Studies have shown that the Y-type ventilation method is an economical and reasonable method to deal with the problem of gas accumulation in the upper corner. It could ensure the safety of coal miners and equipment is guaranteed.

Chen Weimin and Cheng Yuanping believed that the ventilation ratio of Y-type ventilation is determined by the air leakage rate of the working face. They studied the relationship between the main air distribution ratio and the air leakage rate of Y-type ventilation in Chinese coal mines. The studies obtained the gas extraction ratio and ventilation coefficient between the coal seam and the adjacent layer in the coal mine.

The formula of the distribution between the main roadway and the auxiliary roadway is obtained [13]. According to the actual measurement, it is concluded that the air leakage is divided into three areas. They are: the rapid velocity zone, the wind speed gradient zone and the wind speed trending zone.

---

### **1.2.2 Study on the law of gas migration in goaf**

---

The gas problem in the goaf of Chinese coal mines is mainly caused by the coal wall, the residual coal that has fallen, and the leftover coal seam that has not been mined. After a series of studies, foreign scholars believed that coal mine gas is a state of adsorption in coal. At the same time, after a certain degree of diffusion, it will also be converted into a free form. It complies with Darcy's law and Fick's law.

Zhou Shining believes that gas has different physical laws between the newly exposed coal wall and the old coal wall. The gas in the fresh coal wall conforms to Darcy's law. The gas in the old coal wall is in accordance with Fick's law. each

Bai Fasong used numerical simulation to study the problem of gas floating in coal mine goaf. The wind speed distribution is the main influencing factor of gas floating. Because the gas measurement at the coal mine site is difficult and dangerous. So he decided to use the CFD model simulation method. The results show that the airflow pattern in the goaf is consistent with the coal mine site. Therefore, the CFD model is an effective method to study the gas distribution in the goaf [15].

---

### **1.2.3 Gob area gas drainage technology**

---

In the 1930s, the Commonwealth began to extract methane to control its discharge. Japan first pumped the gob after 1934, but the formal industrial extraction gas began in the middle of the 19th century at the German Ruhr coalfield in the Mansfield mine. In 1952, the Soviet Union first extracted gas from adjacent layers in the Red Star mining area of Donbass [16].

China's industrial gas extraction began in the northeastern part of China in the 1930s. In the 1950s, there was a systematic gas drainage work in Longfeng Mine. In 1957, Yangquan became the first city in the vicinity of the gas drainage. From the 1960s to the end of the 1970s, in addition to continuing research on adjacent layer drainage techniques, in the field of gas drainage in China, the related technologies of coal mine low permeability coal seams were further studied [17].

---

## 1.3 Project research content and method

---

### 1.3.1 research content

---

#### (1) Study on gas distribution in gas source and goaf

The gas generation in the working face was studied. According to the gas source separation measurement technology, the gas source has been accurately analyzed, which lays a foundation for optimizing the extraction measures and suppressing the emission of key gas sources. [18-20].

#### (2) Air leakage measurement in goaf

Based on the resistance distribution and pressure energy analysis of the working face area, the possible source and sink of the wind leakage are determined. The combination of instantaneous and steady-state release of SF<sub>6</sub> is used to accurately determine the air leakage velocity, the air leakage and the air leakage channel distribution in the goaf. The law of gas distribution in empty areas lays the foundation [21].

#### (3) Study on the development law of mining fissures

Based on the theory of elastoplastic mechanics and the theory of rock mechanics, the formation process of the "three belts" in the goaf of the fully mechanized caving face is analyzed. Firstly, the mining fracturing zone and the height of the caving zone are analyzed by the theory of mine pressure, and UDEC is applied. Use the finite element simulation software, analyzed the cracks, cracks, caving and separation of the roof of the goaf, and analyzed its changes [39].

#### (4) Numerical simulation of three-dimensional modeling of flow field in goaf

Based on the conditions of the coal seam in the working face and the rock mechanics of the roof rock, combined with the investigation of the mining pressure, geological mechanism state and gas emission conditions of the mining face, the "three horizontal areas" of the goaf based on UDEC numerical software simulation analysis. And the distribution of "vertical three belts", the goaf is simplified into a three-dimensional geometric model. Based on the theory of fluid dynamics and the theory of seepage mechanics of porous media, COMSOL MULTIPHYSICS software is used to simulate the gas concentration field and airflow field distribution in the goaf. The simulation

results verify the air leakage measurement results in the goaf and the gas concentration measurement data in the goaf [1].

---

### **1.3.2 Research methods**

---

After theoretical analysis and numerical simulation. Through the use of numerical simulation software, the internal roof of the coal mine goaf and the rock permeability are proved according to the advancement of the mining operation, and the regularity of the roof of the goaf is changed. And the distribution of "three districts" and "three belts". Data support is provided for further goaf simulation. After the basic information of the goaf is set, the internal flow field of the goaf is simulated with the change of the ventilation system, and the migration law and concentration distribution of the gas in the goaf are further simulated. Finally, the effect of high-drainage lanes was added, and a simulation example of the gas distribution law of the W1310 goaf in Gaohe Coal Mine was obtained.

#### (1) Theoretical analysis

Combined with rock mechanics theory, key layer theory, mining fracture zone theory, porous media seepage mechanics. The combination of simulation experiments and field observations. Discuss the theory of gas migration law in mining fissures and the seepage law of porous media [23].

#### (2) Numerical simulation

Through the use of UDEC and COMSOL numerical simulation software, the rock fall of the coal mine goaf, the void distribution of the goaf, the gas distribution of the goaf and the flow field model of the goaf are proved. Analyze the law of roof failure in the mining process, explore the law of gas migration in the goaf and propose the gas control mode of the Y-type ventilation face along the empty roadway [12].

#### (3) On-site observation

The air leakage of sulfur hexafluoride was measured at different points on the working surface and the air leakage of sulfur hexafluoride was determined along the empty road. Exploring the effects of different air distributions on air leakage in goaf.

---

## **1.4 chapter summary**

---

This chapter discusses the gas emission and air leakage patterns of the working face along the empty coal roadway in a single coal seam. The research status of the research in each country is studied, and the conclusions of the former people in the Y-type ventilation mode, the gas migration law in the goaf and the gas drainage technology in the goaf are discussed. This part provides guidance and direction for the writing of this paper. At the same time, the research content of this article was also determined.

---

## 2 Theoretical Analysis of Gas Migration and Fracture Evolution in Goaf

---

The goaf is usually regarded as a porous medium consisting of a mixture of loose coal and rock. The flow field can be modeled by porous media seepage. Because the pore passages in loose coal and caving strata are very irregular, the flow state of gas in them is very complex. In this paper, the study of gas migration in goaf is based on the following basic assumptions:

- (1) The permeability of goaf does not change with time.
- (2) Because of the randomness of caving rock accumulation in goaf, it is usually impossible to distinguish which direction of pore development is larger, so the caving medium in some part of goaf is regarded as isotropic.
- (3) Linear seepage assumption. Usually the air leakage rate in the goaf is very small, so as to the whole goaf, the gas flow in the goaf as a whole conforms to Darcy's law.
- (4) Gas incompressibility assumption in goaf. Usually, the pressure difference between the two ends of the working face is small, and the air leakage rate in the goaf is very small, so the gas in the goaf can be approximately considered as incompressible gas.
- (5) For convenience, this paper assumes that the fluid viscous coefficients are the same everywhere in the goaf.
- (6) Two-dimensional flow field hypothesis. Generally, the caving height of goaf is very small relative to the length and width of goaf, so the flow field in goaf can be regarded as two-dimensional flow field.
- (7) For the sake of convenience, this paper assumes that the temperature is constant everywhere in the goaf, so this paper will not consider the problem of heat transfer.

---

### 2.1 Porous medium model

---

Porous media refers to a solid containing a large number of holes and cracks. The following points can be used to describe porous media.

- (1) Multiphase substances occupy a part of the space, and at least one phase of the multiphase substances is not solid, they can be gas or liquid phases. Solid phase is called solid skeleton.

(2) Porous media have large surface area because of many internal voids.

(3) At least some of the pores should be connected with each other. The interconnected pore spaces are also called effective pore spaces. In the case of fluid flowing through porous media, unconnected holes can be considered as solid frame parts..

---

## 2.2 Mathematical Model of Gas Migration in Goaf

---

### 2.2.1 Continuity Equation

---

The continuity equation serves any substance of fluid nature [24]. The equation expression of the law of conservation of mass is [25]:

$$\frac{\partial \rho}{\partial t} + \frac{\partial(\rho u)}{\partial x} + \frac{\partial(\rho v)}{\partial y} + \frac{\partial(\rho w)}{\partial z} = 0$$

$\rho$  — Fluid density, kg/m<sup>3</sup>;

$t$  — time, s;

$u$  — X-Directional Partial Velocity, m/s;

$v$  — Y-Directional Partial Velocity, m/s;

$w$  — Z-Directional Partial Velocity, m/s.

Using vector divergence symbols  $div = \partial / \partial x + \partial / \partial y + \partial / \partial z$ , The above formula can be transformed into:

$$\frac{\partial \rho}{\partial t} + div(\rho U) = 0$$

Among them, the velocity vector.

The above formula can remove the time term and the unit of density. Converted to [26]::

$$\frac{\partial u}{\partial x} + \frac{\partial v}{\partial y} + \frac{\partial w}{\partial z} = 0$$



## 2.2.2 momentum conservation equation

The rate of change in momentum of each element in a fluid is the resultant force of all forces acting on that element [27, 28]:

$$\frac{\partial(\rho u)}{\partial t} + \text{div}(\rho u U) = \frac{\partial \sigma_{xx}}{\partial x} + \frac{\partial \sigma_{yx}}{\partial y} + \frac{\partial \sigma_{zx}}{\partial z} + F_x$$

$$\frac{\partial(\rho v)}{\partial t} + \text{div}(\rho v U) = \frac{\partial \sigma_{xy}}{\partial x} + \frac{\partial \sigma_{yy}}{\partial y} + \frac{\partial \sigma_{zy}}{\partial z} + F_y$$

$$\frac{\partial(\rho w)}{\partial t} + \text{div}(\rho w U) = \frac{\partial \sigma_{xz}}{\partial x} + \frac{\partial \sigma_{yz}}{\partial y} + \frac{\partial \sigma_{zz}}{\partial z} + F_z$$

The stresses of  $\sigma_{xx}$ ,  $\sigma_{yy}$ ,  $\sigma_{zz}$  are perpendicular to the three directions of the element x, y and z, respectively.  $\sigma_{yx}$ ,  $\sigma_{zx}$ ,  $\sigma_{xy}$ ,  $\sigma_{xz}$ ,  $\sigma_{yz}$ ,  $\sigma_{zy}$  is the shear stress caused by fluid viscosity, respectively.  $F_x$ ,  $F_y$ ,  $F_z$  is the volume force of a microelement, which is produced by gravity and generally acts in the vertical direction of the Z axis.,  $F_x = 0$ ,  $F_y = 0$ ,  $F_z = -\rho g$ .

For Newtonian fluids [26]:

$$\sigma_{xx} = -p + 2\mu \frac{\partial u}{\partial x} + \lambda \text{div}(U)$$

$$\sigma_{yy} = -p + 2\mu \frac{\partial v}{\partial y} + \lambda \text{div}(U)$$

$$\sigma_{zz} = -p + 2\mu \frac{\partial w}{\partial z} + \lambda \text{div}(U)$$

$$\sigma_{xy} = \sigma_{yx} = \mu \left( \frac{\partial v}{\partial x} + \frac{\partial u}{\partial y} \right)$$

$$\sigma_{yz} = \sigma_{zy} = \mu \left( \frac{\partial w}{\partial z} + \frac{\partial v}{\partial y} \right)$$

$$\sigma_{xz} = \sigma_{zx} = \mu \left( \frac{\partial u}{\partial z} + \frac{\partial w}{\partial x} \right)$$

$\mu$  — Dynamic viscosity,

$\lambda$  — Second viscosity,  $2/3$ .

After collated:

$$\begin{aligned}\frac{\partial(\rho u)}{\partial t} + \operatorname{div}(\rho u U) &= \operatorname{div}(\mu \operatorname{grad}(u)) - \frac{\partial p}{\partial x} + S_u \\ \frac{\partial(\rho v)}{\partial t} + \operatorname{div}(\rho v U) &= \operatorname{div}(\mu \operatorname{grad}(v)) - \frac{\partial p}{\partial y} + S_v \\ \frac{\partial(\rho w)}{\partial t} + \operatorname{div}(\rho w U) &= \operatorname{div}(\mu \operatorname{grad}(w)) - \frac{\partial p}{\partial z} + S_w\end{aligned}$$

The expression of  $\operatorname{grad}() = \frac{\partial()}{\partial x} + \frac{\partial()}{\partial y} + \frac{\partial()}{\partial z}$ ,  $S_u = F_x + s_x$ ,  $S_v = F_y + s_y$ ,  $S_w = F_z + s_z$ ;

$s_x$ ,  $s_y$ ,  $s_z$  is:

$$\begin{aligned}s_x &= \frac{\partial}{\partial x} \left( \mu \frac{\partial u}{\partial x} \right) + \frac{\partial}{\partial y} \left( \mu \frac{\partial v}{\partial x} \right) + \frac{\partial}{\partial z} \left( \mu \frac{\partial w}{\partial x} \right) + \frac{\partial}{\partial x} (\lambda \operatorname{div}(U)) \\ s_y &= \frac{\partial}{\partial x} \left( \mu \frac{\partial u}{\partial y} \right) + \frac{\partial}{\partial y} \left( \mu \frac{\partial v}{\partial y} \right) + \frac{\partial}{\partial z} \left( \mu \frac{\partial w}{\partial y} \right) + \frac{\partial}{\partial y} (\lambda \operatorname{div}(U)) \\ s_z &= \frac{\partial}{\partial x} \left( \mu \frac{\partial u}{\partial z} \right) + \frac{\partial}{\partial y} \left( \mu \frac{\partial v}{\partial z} \right) + \frac{\partial}{\partial z} \left( \mu \frac{\partial w}{\partial z} \right) + \frac{\partial}{\partial z} (\lambda \operatorname{div}(U))\end{aligned}$$

For incompressible fluids,  $s_x = s_y = s_z = 0$

so:

$$\begin{aligned}\frac{\partial(\rho u)}{\partial t} + \frac{\partial(\rho u u)}{\partial x} + \frac{\partial(\rho u v)}{\partial y} + \frac{\partial(\rho u w)}{\partial z} &= \frac{\partial}{\partial x} \left( \mu \frac{\partial u}{\partial x} \right) + \frac{\partial}{\partial y} \left( \mu \frac{\partial u}{\partial y} \right) + \frac{\partial}{\partial z} \left( \mu \frac{\partial u}{\partial z} \right) - \frac{\partial p}{\partial x} + S_u \\ \frac{\partial(\rho v)}{\partial t} + \frac{\partial(\rho v u)}{\partial x} + \frac{\partial(\rho v v)}{\partial y} + \frac{\partial(\rho v w)}{\partial z} &= \frac{\partial}{\partial x} \left( \mu \frac{\partial v}{\partial x} \right) + \frac{\partial}{\partial y} \left( \mu \frac{\partial v}{\partial y} \right) + \frac{\partial}{\partial z} \left( \mu \frac{\partial v}{\partial z} \right) - \frac{\partial p}{\partial y} + S_v \\ \frac{\partial(\rho w)}{\partial t} + \frac{\partial(\rho w u)}{\partial x} + \frac{\partial(\rho w v)}{\partial y} + \frac{\partial(\rho w w)}{\partial z} &= \frac{\partial}{\partial x} \left( \mu \frac{\partial w}{\partial x} \right) + \frac{\partial}{\partial y} \left( \mu \frac{\partial w}{\partial y} \right) + \frac{\partial}{\partial z} \left( \mu \frac{\partial w}{\partial z} \right) - \frac{\partial p}{\partial z} + S_w\end{aligned}$$

### 2.2.3 Component transport equation

This study explores the distribution of gas flow in the goaf, so the gas in the goaf can be regarded as a mixture of air and gas. In this way, the fluid composition of seepage fluid changes, so it is necessary to consider the change of gas composition in the goaf [29, 30].

The law of conservation of mass can be expressed as (no chemical reaction):

$$\frac{\partial(\rho c_s)}{\partial t} + \operatorname{div}(\rho U c_s) = \operatorname{div}(D_s \operatorname{grad}(c_s)) + S_s$$

$c_s$  — Gas concentration for a component;

$U$  — Fluid Vector Velocity;

$D_s$  — Dispersion Coefficient of Gas;

$S_s$  — Source term.

Gas transport equation:

$$\frac{\partial(\rho c_t)}{\partial t} + \text{div}(\rho U c_t) = \text{div}(J_t \text{grad}(\rho c_t)) + S_t$$

$$c_t = \phi \rho$$

$S_t$  — Gas source term;

$c_t$  — Gas concentration;

$\phi$  — Voidage;

$J_t$  — Gas dispersion flux;

$U$  — Average seepage velocity;

When the air flow is in the state of high-speed seepage. The gas diffusion flux is [26]:

$$J_t = \left( D\rho + \frac{\mu_t}{Sc_t} \right) \text{grad}(c_t U)$$

$D$  — Gas dispersion coefficient;

$Sc_t$  — Turbulent Schmidt Number;

$U$  — Seepage vector velocity.

When the air flow moves in the underground goaf, it is in the low-speed seepage state. Gas is laminar flow and gas diffusion flux is:

$$J_t = D\rho \text{grad}(c_t U)$$

Gas seepage velocity in goaf of coal mine:

$$u = -\frac{K}{\mu} \nabla p$$

$p$  — pressure;

$K$  — permeability;

$\mu$  — Gas viscosity.

Bring the above process into (2.26). The continuity equation under laminar and turbulent conditions can be obtained:

Laminar flow:

$$\frac{\partial(\rho_t)}{\partial t} + \text{div}\left(-\rho_t \frac{K}{\mu} \nabla p\right) = \text{grad}\left(D\rho \text{div}(c_t U) \frac{K}{\mu} \nabla p\right) + S_t$$

turbulence:

$$\frac{\partial(\rho_t)}{\partial t} + \text{div}\left(-\rho_t \frac{K}{\mu} \nabla p\right) = \text{grad}\left[\left(D\rho + \frac{\mu}{Sc_t}\right) \text{div}(c_t U) \frac{K}{\mu} \nabla p\right] + S_t$$

According to (2.30), mine gas is in goaf. The momentum conservation equation in the coordinate system of direction I is [26]:

$$\frac{\partial(\rho u_i)}{\partial t} + \frac{\partial(\rho u_i u_j)}{\partial x_j} = \frac{\partial(\tau_{ij})}{\partial x_j} - \frac{\partial p}{\partial x_i} + \rho g_i + F_i$$

$$\tau_{ij} = \left[ u_{eff} \left( \frac{\partial u_i}{\partial x_j} + \frac{\partial u_j}{\partial x_i} \right) - \frac{2}{3} \frac{\partial u_i}{\partial x_j} \delta_{ij} \right]$$

$\tau_{ij}$  — Stress tensor;

$g_i$  — Volumetric force in direction I;

$u_{eff}$  — The sum of hydrodynamic viscosity and turbulent viscosity;

$\delta_{ij}$  — Kroneker Mark;

$F_i$  — Custom Source Items.

so:

$$\frac{\partial(\rho u_i)}{\partial t} + \frac{\partial(\rho u_i u_j)}{\partial x_j} = \frac{\partial}{\partial x_j} \left( u_{eff} \frac{\partial u_i}{\partial x_j} \right) + \frac{\partial}{\partial x_j} \left( u_{eff} \frac{\partial u_j}{\partial x_i} \right) - \frac{2}{3} \frac{\partial}{\partial x_j} \left( \frac{\partial u_i}{\partial x_j} \right) - \frac{\partial p}{\partial x_i} + \rho g_i + F_i$$

$$Q_i = \frac{\partial}{\partial x} \left( u_{eff} \frac{\partial u_j}{\partial x_i} \right) - \frac{2}{3} \frac{\partial}{\partial x_i} \left( \frac{\partial u_j}{\partial x_j} \right) + F_i$$

$$F_i = \sum_{j=1}^3 D_{ij} u_{eff} q_j + \sum_{j=1}^3 C_{ij} \frac{1}{2} \rho |q_j| q_j$$

The momentum conservation equation in the three directions of x, y and Z is:

$$\frac{\partial(\rho u_x)}{\partial t} + \frac{\partial(\rho u_x u_j)}{\partial x_j} = \frac{\partial}{\partial x} \left( u_{eff} \frac{\partial u_x}{\partial x_j} \right) - \frac{\partial p}{\partial x} + Q_x$$

$$\frac{\partial(\rho u_y)}{\partial t} + \frac{\partial(\rho u_y u_j)}{\partial x_j} = \frac{\partial}{\partial x} \left( u_{eff} \frac{\partial u_y}{\partial x_j} \right) - \frac{\partial p}{\partial y} + Q_y$$

$$\frac{\partial(\rho u_z)}{\partial t} + \frac{\partial(\rho u_z u_j)}{\partial x_j} = \frac{\partial}{\partial x} \left( u_{eff} \frac{\partial u_z}{\partial x_j} \right) - \frac{\partial p}{\partial z} + \rho g_z + Q_z$$

---

### 2.3 Summary of this chapter

---

In this chapter, through the existing theory and a series of deductions, the properties and basic parameters of porous media in goaf are obtained. According to the theory of fluid mechanics, the movement equation of gas in goaf is discussed. Based on the existing experience and knowledge, the division of "vertical three generations" and "horizontal three zones" in goaf and their respective properties are explored.



---

### **3 Study on Numerical Simulation of gas migration in goaf of mining fissures and Y-type ventilation system**

---

The law of gas migration in goaf has always been the focus and difficulty of gas prevention and control in coal mine. The field work of gas migration research in goaf is to extract the gas in goaf and make component analysis. Now through computer simulation, the process of gas migration in goaf under different ventilation modes and seepage conditions can be described theoretically. Quantitative and regular conclusions can be obtained on the computer by changing the boundary conditions or system parameters manually. And then formulate control measures to prevent the occurrence of gas disasters in goaf [38-40].

---

#### **3.1 Overview of working face**

Gaohe Coal Mine is located 4km west of Changzhi City in Shanxi Province and is affiliated to Lu'an Mining Group. The W1310 working face is located in the south-central area of Xitian District of Jingtian. The working face is 1530m long, 320m wide and the average inclination angle is 8°. The mining method is adopted, and the fully mechanized top coal mining process and the roof are completely collapsed. The W1310 working face is located in No. 3 coal seam of Gaohe Mine, and its roof is mainly composed of mudstone, sandy mudstone, argillaceous duststone, siltstone, fine-grained sandstone, medium-grained sandstone and coarse-grained sandstone. The direct top is argillaceous rock with a thickness of 0~11.8m, and the old top is sandstone with a thickness of 8.05m.

---

#### **3.2 Standard goaf seepage model**

For a standard goaf, it can be considered as a cube model with a strike as the X-axis, a tendency to the Y-axis, and a longitudinal Z-axis. In general, the goaf is characterized by a large size in the XY plane, and a small Z-direction height relative to the goaf. Most of the coal is concentrated in the bottom of the goaf, and the height is about 20cm. Therefore, for the study of spontaneous combustion of residual coal in the goaf, the goaf is regarded as a two-dimensional rectangular plane, and the permeability is subject to two-dimensional distribution. For the problem of gas migration, because the gas density is lower than that of air, there is a floating effect under the condition of low flow velocity in the goaf, and there is a certain difference in

the longitudinal distribution. Therefore, when studying such problems, the gob is often used. Think of it as a three-dimensional cuboid.

### 3.2.1 Empirical Model of Void and Permeability

Take the intersection of the wind lane and the work surface as the coordinate origin. The direction of the goaf is the positive X direction, and the direction of the goaf is the positive Y direction. The empirical formula for the porosity of coal mine goaf is [42]:

$$n_x = 0.2e^{-0.0223x} + 0.1$$

$n_x$ —The size of voidage along X-axis in Goaf;

$x$ —The coordinate value in the direction of goaf strike.

$$n_y = e^{-0.15\left(\frac{L+y}{2}\right)} + 1$$

$n_y$ —The size of voidage along Y axis in Goaf;

$y$ —Coordinate value of direction of goaf;

$L$ —Tendency length of goaf.

Two-Dimensional Distribution of Void Rate in Goaf of Coal Mine:

$$n = n_x \cdot n_y = \left(0.2e^{-0.0223x} + 0.1\right) \cdot \left(e^{-0.15\left(\frac{L+y}{2}\right)} + 1\right)$$

Wang Yuehong [59] and others believe that the relationship between porosity and permeability in goaf of coal mine is consistent:

$$K = 1.605e^{-6} \cdot n^2$$

The curve is shown in Figure1.。

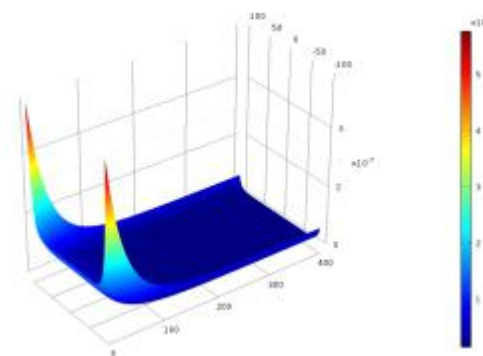


**Figure 1 Empirical Model Permeability Distribution**



After a series of laboratory experiments, the relationship between voidage and permeability is expressed as follows.:

$$K = 2 \times 10^{-6} \cdot e^{3.23x}$$

Based on the above formulas, the permeability equation of the goaf is obtained as follows.

$$K = 2 \times 10^{-6} \times e^{(0.2e^{-0.0223x} + 0.1) \left( e^{-0.15(\frac{L}{2} \pm y)} + 1 \right)}$$

The corresponding distribution is shown in Figure 2. .

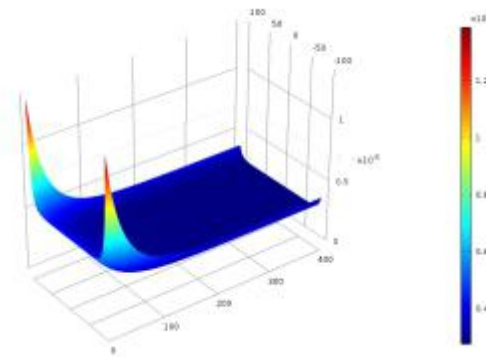


**Figure 2 Empirical Model Permeability Distribution**

Carman equation holds that the distribution of permeability and voidage in goaf obeys the relation.:

$$K = \frac{K_0}{0.241} \left( \frac{n^3}{(1-n)^2} \right)$$

$K_0$ ——Initial permeability value;

$n$ ——Voidage. .

Comprehensive empirical formula of void fraction. The permeability formula of goaf is obtained as follows.:

$$K = 6.23 \times 10^{-6} \times \left( \frac{(0.2e^{-0.0223x} + 0.1)^3 \cdot \left( e^{-0.15(\frac{L}{2} \pm y)} + 1 \right)^3}{\left[ 1 - (0.2e^{-0.0223x} + 0.1) \cdot \left( e^{-0.15(\frac{L}{2} \pm y)} + 1 \right) \right]^2} \right)$$

The permeability distribution of mined-out area corresponding to this formula is shown in Fig. 3

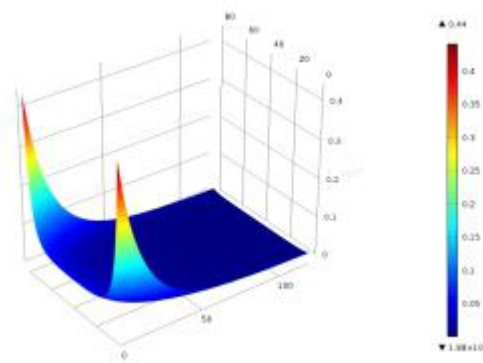


Figure 3 Empirical Model Permeability Distribution

### 3.2.2 Three-dimensional permeability model

Based on the "O" ring theory proposed by Academician Qian Minggao, Chen Peng established a three-dimensional permeability model. Figure 4 shows [43-45].

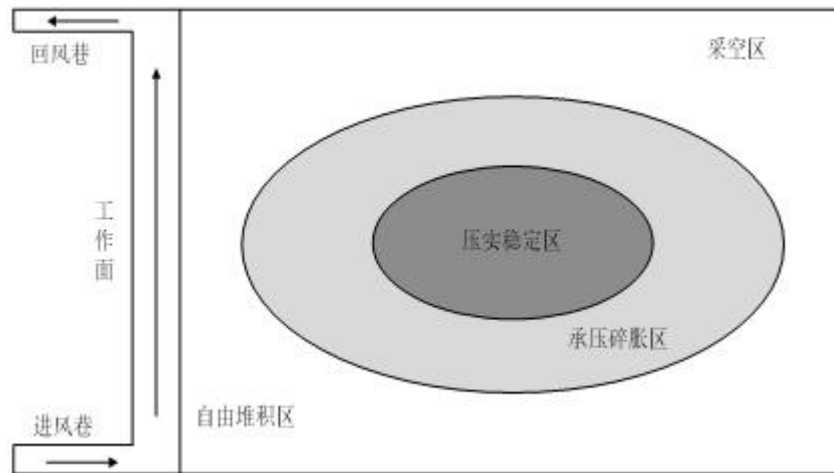


Figure 4 Theoretic schematic diagram of O-ring

The main point of air leakage is the peripheral fracture development zone. The middle part of the goaf has the lowest porosity and the lowest permeability, while the periphery has the highest permeability. The equation is:

$$n = n_x \cdot n_y = (0.2 \times e^{-0.02223 \left( \frac{D}{2} - \left| \frac{D}{2} - x \right| \right)} + 0.1) \cdot (e^{-0.15 \left( \frac{L}{2} - |y| \right)} + 0.1)$$

D——Strike length of goaf;

L——Tendency length of goaf

At the same time, in the vertical direction, "O" theory divides the goaf into three different parts.

The outermost circle is free accumulation area, and the void fraction is exponentially high and low.

In the inner compacted zone, the change of porosity is small, and the pressure in the central part is the largest, which is the fragmentation and expansion zone. Overall, smooth transition processing can be done. If the void change rate in the vertical direction is set to be 1, then the change coefficient NZ can be expressed as [26,46]:

$$n_z = \begin{cases} 1.01^z, & \left(\frac{x-\frac{D}{2}}{a_2^2} + \frac{y^2}{b_2^2}\right) \geq 1 \\ \left[ \frac{4 \cdot \left(x-\frac{D}{2}\right)^2}{a_1^2} + \frac{y^2}{b_1^2} \right]^{-0.007178z}, & \frac{1}{4} < \left(\frac{x-\frac{D}{2}}{a_2^2} + \frac{y^2}{b_2^2}\right) < 1 \\ 1, & \left(\frac{x-\frac{D}{2}}{a_2^2} + \frac{y^2}{b_2^2}\right) \leq \frac{1}{4} \end{cases}$$

According to the comprehensive empirical formula, the three-dimensional permeability distribution formula of goaf is as follows:

$$K = 1.605 \times 10^{-6} \cdot (n_x \cdot n_y \cdot n_z)^2$$

From the above study of empirical formula, we can draw a conclusion that on the basis of "O" circle theory, the variation and different properties of porosity in vertical direction at different locations in underground goaf are analyzed and utilized, and the result is more scientific and reasonable [26].

---

### 3.3 Numerical simulation of mining fissure evolution

---

#### 3.3.1 Introduction to UDEC Numerical Simulation Software

---

UDEC numerical simulation software is a two-dimensional discrete element program for processing discontinuous media. Therefore, it is an ideal tool for simulating discontinuous feature damage models. UDEC is commonly used in mining projects.

### 3.3.2 Establishment of UDEC numerical model

In this paper, the Y-type working face of Gaohe Coal Mine is taken as the basic prototype, and the numerical simulation of pore fissure evolution in goaf is carried out. According to the investigation, the average thickness of the coal seam of the Y-type working face is 5m, the strike length is 1500m, the inclination length is 305m, the working surface inclination angle is 15~18°, the mining height is 5m, and the average mining speed is 5 m/d. The rock formation above the model is dominated by sandstone with a height of 200m and a bulk density of 16 KN/m<sup>3</sup>. The model is not added in the simulation and is treated by equivalent load. The equivalent load is calculated as [26, 47]:

$$q = \sum \gamma H$$

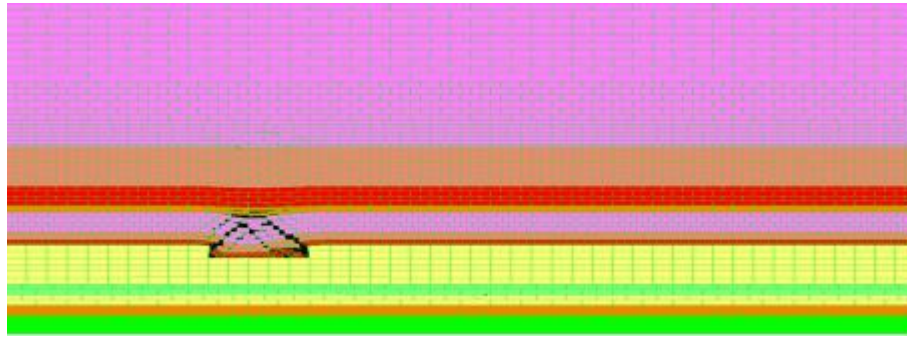
$\lambda$  ——Average Volume Weight of Unsimulated Overburden Strata, N/m<sup>3</sup>;

$H$  ——Thickness of Unsimulated Rock Bed above Coal Seam, m。

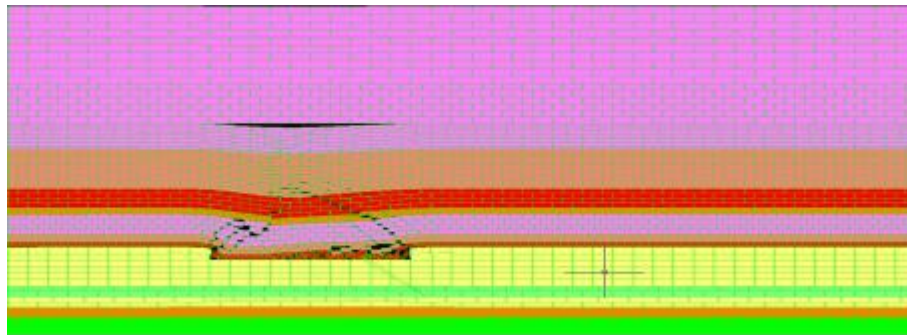
The simulation results are shown in Figure 5.

**Table 2 Table of mechanical parameters of UDEC simulated strata**

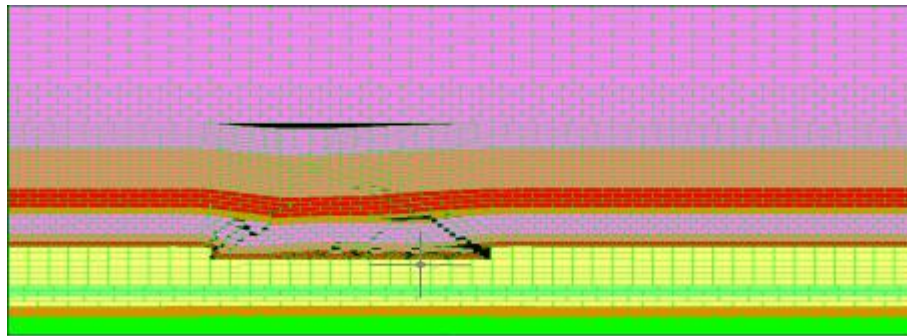
No.	Rock property	thick (m)	density (g/cm <sup>3</sup> )	Bulk modulus (GPa)	shear modulus (GPa)	Friction angle (°)	Cohesion (MPa)	Tensile strength (MPa)
J1	Siltstone	11.2	2.5	6	9	29	31	12
J2	Siltstone	8.13	2.5	41	29	53	15	2.6
J3	Sandstone	7.4	2.7	25	15	41	29	24
J4	pelitic siltstone	12	2.5	9	8	32	34	12
J5	Mudstone	61.2	2.8	45	39	60	41	32
J6	Siltstone	19.21	2.7	26	12	42	29	24



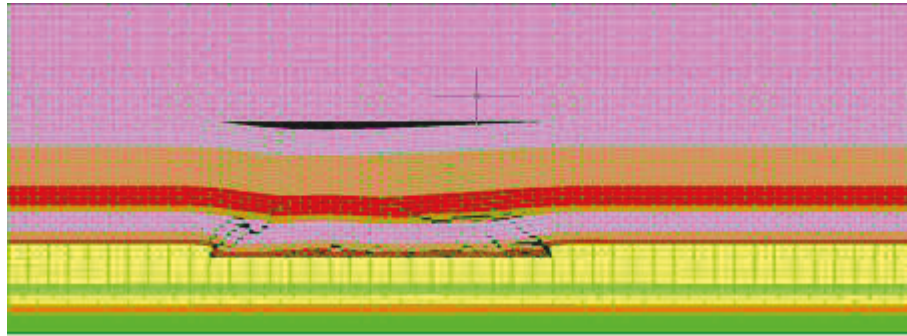
(a) 50m



(b) 100m



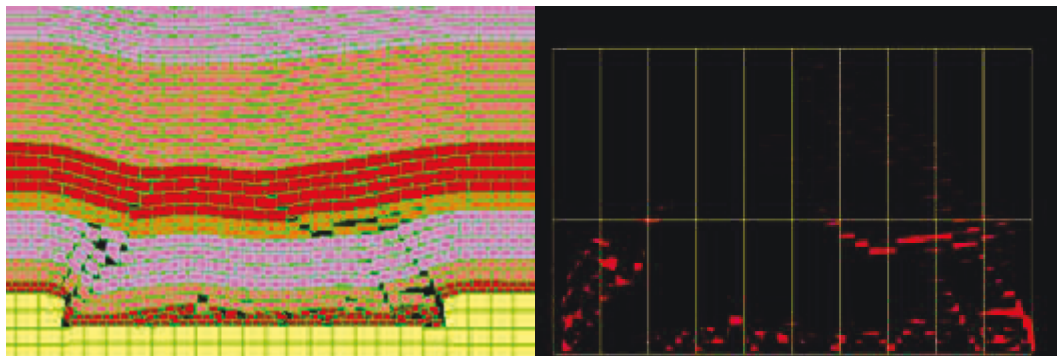
(c) 150m



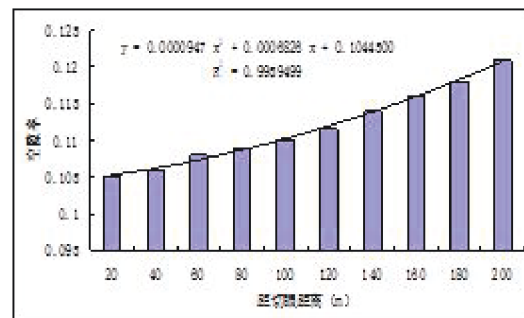
(d)200m

**Figure 5 UDEC simulation results**

As time goes by and the work surface advances, the simulation results are getting closer and closer to our theoretical analysis. Meet the description of the O-ring theory. Count one unit every 20 meters, and the layout and variation law of the caving zone and the fracture zone of the coal mine goaf are simulated. The distribution curve is fitted, as shown in Figure 6.



(a) Development of cracks in 200 m (b) Fracture map processing and zoning



(c) Caving zone voidage statistics (d) Fracture zone voidage statistics

**Figure 6 Vacancy distribution in Goaf**

As shown in Fig. 6 (c), the void fraction is relatively high at 180 to 200 m under the support force. The stress transition zone is 120 to 180 m, and the void fraction of this part changes from high to low. In the re-compacted zone of 40 to 80 m, the void

fraction is approximately equal to 0.15. At 20m, the void fraction increases [26] because of the support force.

On the strike of W1310 working face, the influence length of coal wall on porosity is about 20m, and the transitional zone is about 60m. The void fraction of the fractured zone is about 0.104~1.21, with little change. Therefore, it is assumed that the fixed value is 0.11. According to the theory of "O" type circle, the distribution of porosity is basically the same in tendency and trend, the main reason is the supporting effect of coal wall.

Formula is used to calculate the relationship between porosity and permeability in mined-out area, and the permeability model is obtained as shown in Figure 7.

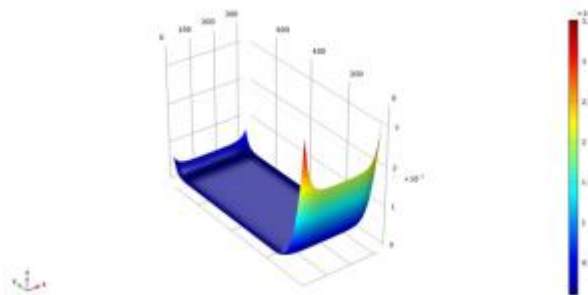


Figure 7 Permeability Model of Caving Zone in Goaf

---

### 3.4 Summary of chapter

---

According to the theoretical analysis of the lithology of the goaf, the permeability model of the goaf is simulated in this chapter. UDEC software is used to simulate the evolution law of mining fissures and explore the distribution of three zones in the goaf. The permeability model of goaf is obtained by synthetically fitting the distribution curve and "O" circle theory. It lays a foundation for the establishment of goaf model.





---

## 4 Study on Numerical Simulation of gas migration in goaf of Y-type ventilation system

### 4.1.1 Introduction to COMSOL Software

COMSOL Multiphysics is a relatively popular numerical simulation software at this stage. It will be seen in various engineering applications with multiple physical quantities coupling. As a CFD software, it has the advantages of simple and convenient operation, neat and tidy interface, accurate and reasonable simulation results.

---

### 4.1.2 Establishment of COMSOL physical model

The data provided by Gaohe Coal Mine and measured by field workers set up the model parameters. Each inlet tunnel and gob-side retaining roadway is 4 m wide and 3.2 m high; the thickness of flexible membrane wall is 3 m, the working face is 5 m wide and 3.2 m high; the goaf is 750 m and tends to 320 M. The caving and fracture zones are 30 m and 35 m high respectively. The coordinate origin is the lower corner of the working face. The model is shown in Figure 8. of the working face. The model is shown in Figure 8.

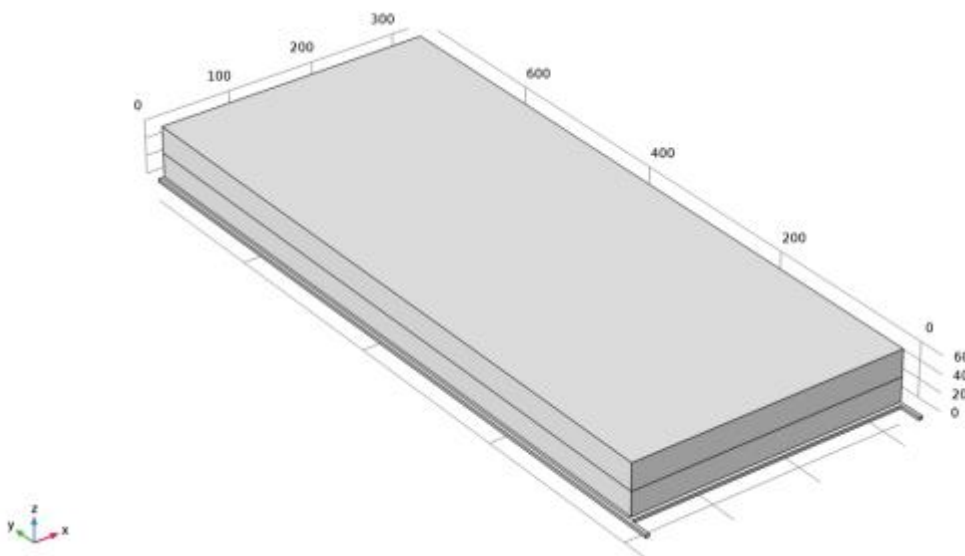


Figure 8 Y Working Face Model

---

### 4.1.3 Boundary Conditions Setting

---

The main and auxiliary air intake are set at 3200 m<sup>3</sup>/min and 700 m<sup>3</sup>/min respectively. The main air intake is 3.78 m/s and the secondary air intake is 0.91 m/s. The end of gob-side entry retaining is set as the end of wind. The internal parameters of mine goaf are set as multi-void medium. The flexible membrane wall is porous media with permeability of 1e-10m<sup>2</sup>. The rest is set to the boundary. [26].

---

## 4.2 simulation results analysis

---

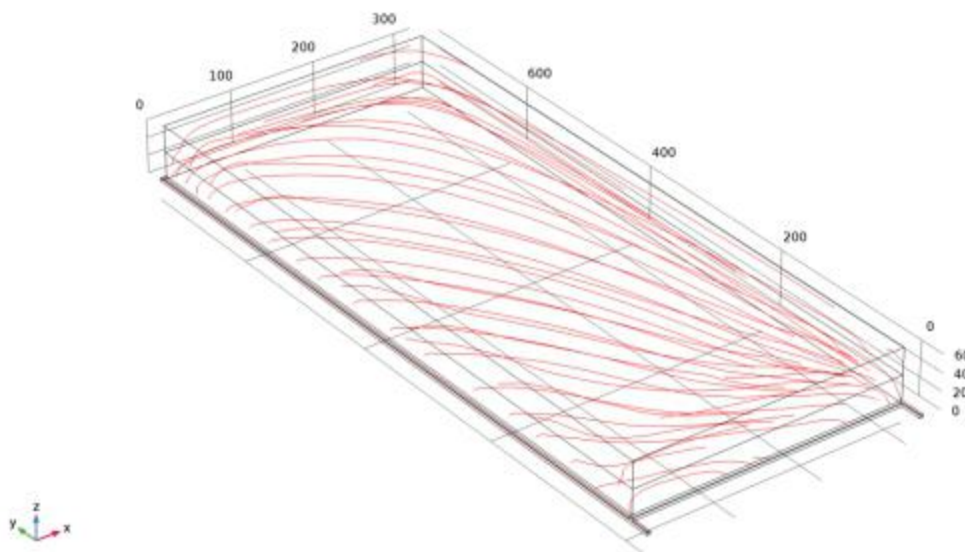


**Figure 9 Wind Trajectory**

Figure 9 is the airflow trajectory curve of goaf. It can be seen from the graph that the airflow characteristics of goaf have an important influence on the law of gas migration. Streamline density of caving zone in goaf is larger than that of fissure zone. Among them, the streamline in the edge of the caving zone is denser and the middle part is sparse, which is caused by the "O" type distribution of the voids in the goaf. According to the breaking rule of the goaf roof, the central part of the goaf is compacted, the void ratio is small, and the air flow resistance is large; because of the support of the coal wall, the edge has large void ratio, small air flow resistance, large amount of air leakage and large air leakage velocity [48].

From Figure 10, it can be seen that the gas concentration in goaf increases gradually from working face to goaf. The main air intake and the secondary air intake gradually decrease.

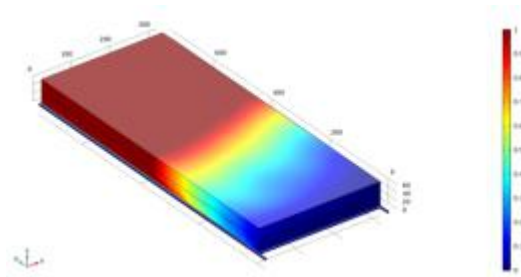


**Figure 10 Overall Gas Distribution in Goaf**

#### 4.2.1 Vertical Direction of Goaf

From Fig. 11, it can be seen that at the height of  $z=1.5\text{m}$ , the gas concentration in the deep goaf increases gradually from the working face. The main reason is that air leakage has migration effect on gas distribution. The smaller the wind speed, the smaller the influence of gas flow on gas migration.

Gas concentration increases near gob-side retaining roadway, Because the air flow from the auxiliary intake lane into the goaf has a large air pressure and a large air leakage. After that, the two air inflows converge and flow out along the goaf retaining roadway. Therefore, along the side of goaf retaining roadway, the area of low gas concentration gradually narrows [49-51].

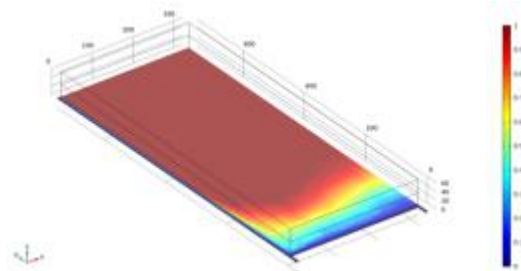


**Figure 11  $z = 1.5\text{ m}$  gas distribution**

As can be seen from Figure 12. The gas distribution is almost the same when it is 1.5m and 10m away from the bottom of goaf. They are all close to the side of gob-side retaining roadway. However, the overall gas concentration in goaf is relatively low at 10m, and the gas concentration near the working face is increased.

Because the work faces the goaf with high air leakage, it affects the gas in the goaf 10 m high.

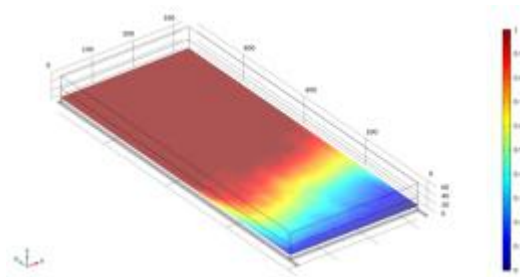


**Figure 12 z = 10m gas distribution**

From Fig. 13, it can be seen that the level of  $Z = 32\text{m}$  at the bottom of goaf. The gas concentration increases gradually from the intake side to the side of gob-side retaining roadway. It can be said that the phenomenon of air leakage in goaf has no effect on several parts of gas distribution in goaf at higher position. The high gas concentration in the back of goaf is due to the high degree of compaction, small air leakage and the buoyancy of gas in the lower caving zone. So it is full of the upper falling zone space [52].

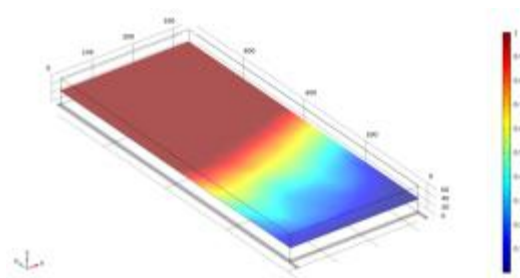


**Figure 13 z = 32m plane gas distribution**

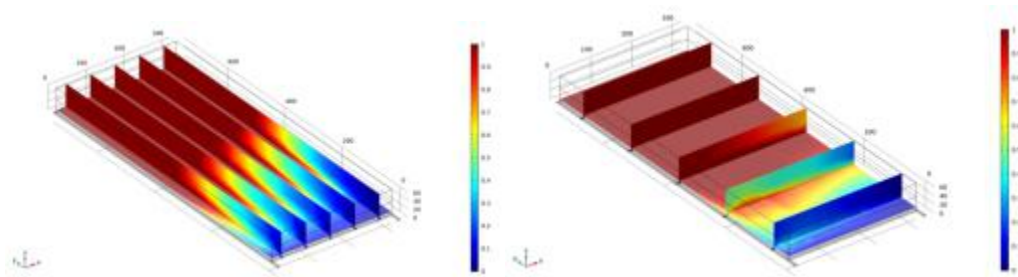
#### 4.2.2 Direction of Vertical Working Face

It can be seen from Figure 14 The gas concentration in the side of goaf near the working face rises first and then decreases. Because on the intake side, the air flow directly enters the goaf at the position of the belt groove. The gas here is diluted by fresh air, and the gas concentration is low. At a later distance, eddy currents appear in the working face. The difference of air pressure drives gas to flow back to the working face from the goaf, so the gas concentration here rises. After that, the air flow gradually stabilized in the working face stage, and the gas flowed back to the goaf again because of the pressure effect, and the gas concentration in the goaf decreased.

On the other side of the intake tunnel, the gas concentration increases but the pressure decreases. Because the rock falling in the goaf is compacted and the void

ratio is small, the phenomenon of air leakage is difficult. Gas transport here is almost unaffected [53, 54].

Because the concentration of methane is lower than that of air, a large number of gas in goaf will float into the fissure zone, while the fissure zone in goaf has a small void rate and a very small air leakage speed, which can not effectively take away the gas, resulting in a high gas concentration in the fissure zone. Therefore, it is necessary to take reasonable measures to control the gas in the fissure zone of goaf [55].



(e) Gas Concentration Trend Profile (f) Gas Concentration Tendency Profile

**Figure 14 Gas Profile of Goaf**

### 4.2.3 Numerical simulation results under high pumping conditions

In order to study the effect of high-drainage control on the Y-type working face of Gaohe Coal Mine, the model shown in Figure 15 was established. Among them, the vertical height of the high pumping lane is 32 meters from the bottom plate, the horizontal position is 40 meters away from the return air lane, and the fixed exhaust air volume of the high pumping lane is 400 m<sup>3</sup> / min.

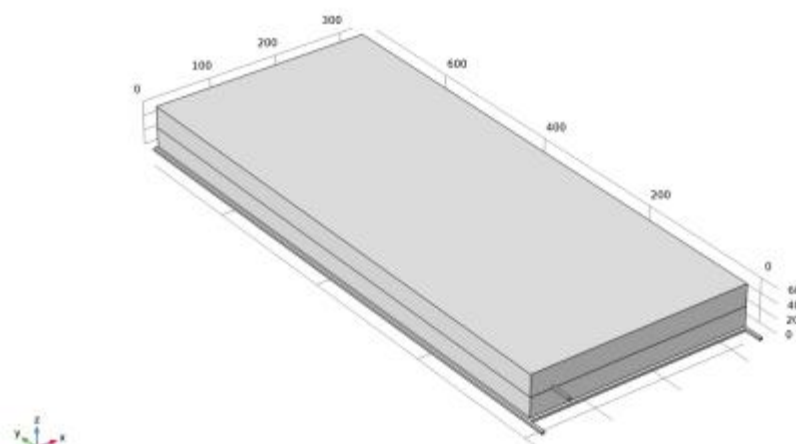


**Figure 15 Gas Control Model of High Drainage Roadway**

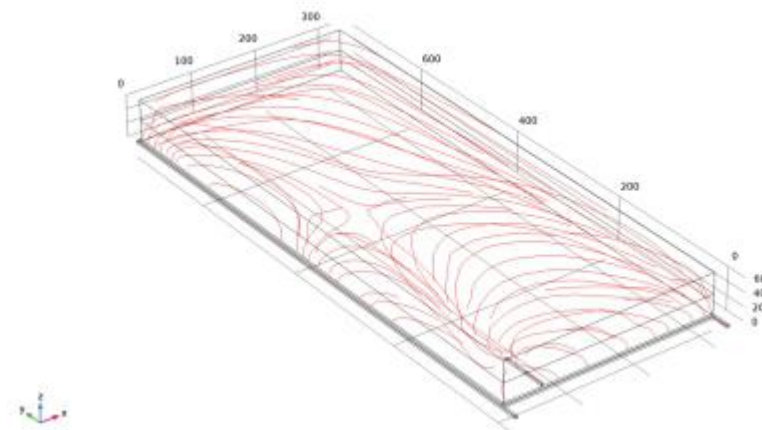


**Figure 16 Air flow trajectory in goaf under high pumping condition**

Figure 16 shows the airflow trajectory in the goaf under the condition of high extraction roadway opening. Comparing the results, it can be seen that the air flow trajectory inside the goaf has changed significantly due to the drainage effect of the high-level extraction roadway. A large amount of air flow in the half part of the goaf is withdrawn from the high extraction roadway, only the latter part of the air flow in the flexible membrane wall leaks back to the goaf retaining roadway.

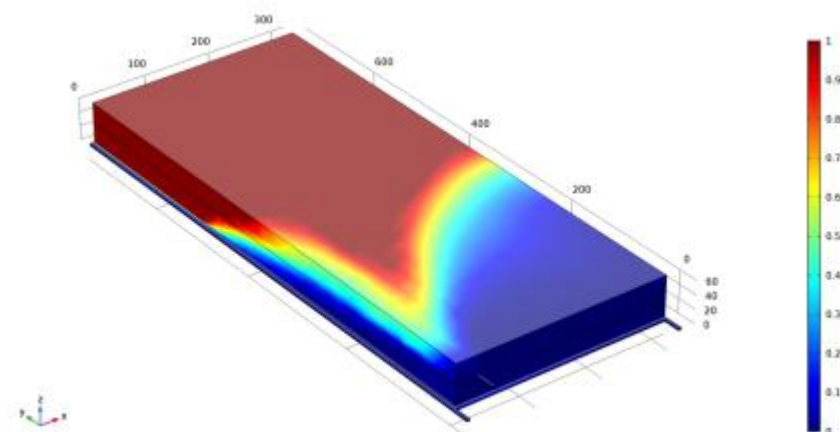


**Figure 17 Gas distribution in Goaf**

Figure 17 shows the overall distribution of gas in goaf under the condition of high extraction roadway. It can be clearly seen from the graph that under the extraction of high-concentration gas in the fissure zone, the high-concentration area shifts to the side of the gob-side retaining roadway, and a high-concentration triangle area appears. Because of the drainage effect of high drainage roadway, the gas concentration in the caving zone of goaf has changed, especially in the high gas concentration area which near the flexible membrane wall.

---

### **4.3 Summary of this chapter**

---

COMSOL software was used to simulate the flow field distribution in the goaf, and the gas concentration distribution in the goaf under different conditions was found out. Under the action of high extraction roadway, the air flow trajectory inside the goaf has changed greatly due to the drainage effect of high extraction roadway. A large amount of air flow in the goaf is withdrawn from the high extraction roadway, only the latter part of the air flow in the flexible membrane wall leaks back to the goaf retaining roadway. It can play a guiding role for gas prevention and control in goaf in the future.





---

## 5 Analysis and Measurement of Air Leakage Law of Fully Mechanized Caving Face

---

The distribution of the air leakage passages in the goaf and the air leakage intensity not only affect the effect of gas drainage in the goaf, but also affect the spontaneous combustion characteristics of the residual coal in the goaf. Therefore, it is very important to quantitatively measure the amount of air leakage in the goaf and determine the corresponding air leakage distribution. At the same time, the ventilation network is in a dynamic state in the mine. Changes in the ventilation network structure and branch wind resistance will have a certain impact on the size and direction of the wind flow. This will also have an impact on the air leakage distribution in the goaf. That is to say, with the progress of mining work, the structure and wind resistance of the ventilation network will change accordingly, and the wind flow in the wind network will also change. Therefore, by measuring the resistance of the mining area, a ventilation network affecting the production working surface is established. The calculation model provides a reference for the analysis of the air leakage caused by the differential pressure of the working face and the relative pressure change along the empty roadway for future design and analysis [52].

---

### 5.1 Y-type working face pressure energy analysis

---

#### 5.1.1 Barometer method

---

Refers to the use of a precision barometer to measure the relative static pressure difference between the two measuring points. Together with the dynamic pressure difference and the potential energy difference, the ventilation resistance of the system is obtained [53].

Known by the energy equation:

$$h_{12} = (P_1 - P_2) + \rho_{12} g Z_{12} + \left( \frac{1}{2} \rho_1 v_1^2 - \frac{1}{2} \rho_2 v_2^2 \right)$$

Where  $\rho_{12}$  is 1, 2 is the average density of different gas fractions between the two sections.

For the 1 and 2 parts, the relative static pressures  $P_1$  and  $P_2$  are measured by a precision barometer; and the average wind speeds  $v_1$ ,  $v_2$  are measured with a wind

gauge; the temperatures  $t_1$ ,  $t_2$  and relative humidity  $\phi_1$ ,  $\phi_2$  are measured with a dry and wet thermometer. Then, the air density value  $\rho$  of each section is obtained from the respective  $P$ ,  $t$ , and  $\phi$  values of the two sections. If the height difference between the two sections is not large, then the density  $\rho_{12}$  of the air column between the two sections can be approximated; if the height difference between the two parts is large, the air density should be divided into several parts to calculate two The potential difference between the parts.

When two points are measured using a precision barometer. Due to the inconsistency of time, the surface atmosphere will also change accordingly. Therefore, the accuracy of the measurement will not be guaranteed. In this case, we can use the base point method or the synchronization method to avoid these errors perfectly [53].

#### (1) Synchronization method

Synchronization is the simultaneous reading of two people who measure different points downhole. This method can effectively avoid the error caused by atmospheric pressure due to different time. However, the tacit agreement between the two people is too high and inefficient. Therefore, less use [54, 55].

#### (2) Base point method

The base point method measures the change in airflow pressure by using a precision barometer at a preset base point, while another precision barometer measures the relative static pressure of each mine.

The base point method is characterized by time savings, effortlessness, and speed in measuring ventilation resistance. In the process of using the base point method, we should pay attention to the following points [56]:

- (1) The surveyor needs to accurately record the elevation of the test location;
- (2) The measurement needs to be completed in the inspection workshop;
- (3) In order to avoid airflow interference. Multiple base point measurements can be taken.

---

### 5.1.2 Analysis of Pressure Energy Distribution in Working Face

---

When measuring points are laid out on the working face, in order to conveniently count the distance between the measuring points and the lower corner, the distance is determined by counting the number of hydraulic support numbers. For the gob-side

retaining roadway, the distance is determined by inquiring the number of flexible membrane wall masonry. Seven points are tested on the working face and ten points are tested on the gob-side retaining roadway. The base points are arranged in the upper corner of the working face, and the pressure measurement results are in accordance with the above mentioned. After eliminating the influence of potential pressure difference and atmospheric pressure, the method is treated as shown in Table 3 and Fig. 18 and Fig. 19.

**Table 3 Distribution Table of Relative Pressure of Air Flow in Working Face**

Direction Length of Inlet Air Flow in Working Face /m	Relative pressure /Pa	The distance between gob-side entry retaining and upper corner /m	Relative pressure /Pa
0	659	0	586
60	637	150	468
120	610	225	456
180	595	300	415
240	583	400	361
300	581	450	314
305	578	600	217
		750	163
		900	20
		1050	0

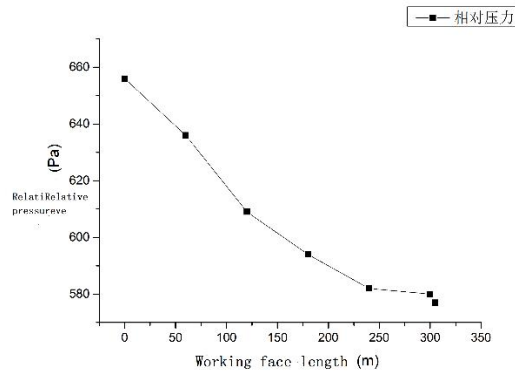


**Figure 18 Relative Pressure Distribution Diagram of Air Flow in Working Face**

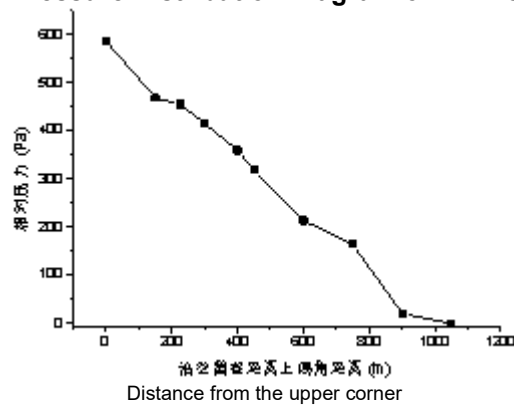


**Figure 19 Retaining Roadway along Gob**

Because the friction coefficient at different positions of the working face can be considered to be basically the same. Therefore, according to the ventilation resistance formula  $H = RQ^2$ , if the face does not leak to the goaf or the goaf does not leak to the working face, the pressure drop of the working face should be linear.

Through the analysis of Fig. 18, it can be seen that the pressure drop of the working face slows down gradually from the lower corner of the cut hole to 250 M. It shows that the air volume of the working face decreases gradually, and the direction of air leakage in the working face is the air leakage in the goaf. The air pressure of the working face from 250 m to 305 m is basically stable. Therefore, it can be judged that this part does not leak to the goaf, the goaf does not leak to the working face, and most of the air leaks from the high extraction roadway and the goaf to the goaf retaining roadway along the goaf are the air leaks to the goaf within 250 meters of the working face. Therefore, the Y-type working face ventilation system has greatly changed the air leakage flow field in goaf.

Through the analysis of Fig. 19, it can be seen that the change of relative pressure drop slope in gob-side retaining roadway is relatively gentle. According to theoretical analysis, if the resistance property of gob-side retaining roadway is basically the same, the air leakage in gob-side retaining roadway increases gradually with the air leakage from gob-side retaining roadway. Therefore, the pressure drop slope should be gradually increased, but due to the bottom heave of gob-side retaining roadway and the correction reasons of position pressure difference. It is unavoidable that there are errors in measurement results, but it can still be found through measurement results that the maintenance quality of gob-side entry retaining is better and the air leakage rate is the same.

---

## **5.2 Work surface leakage measurement**

---

### **5.2.1 Tracer gas method for measuring the principle of air leakage**

---

For Y-type ventilation, the working face extension is continuous positive pressure leakage, as shown in Figure 20. Therefore, a continuous release point, R1, R2, ..., Rn, must be arranged in the direction of the incoming air. Thereafter, SF6 gas was discharged at a constant rate  $q$  (m<sup>3</sup>/min) at each point. Because of the air leakage, the amount of wind along the way will be less and less. Then the concentration of SF6

will continue to increase. Therefore, the obtained SF6 concentration is a ladder rise [57].

The concentration of SF6 at the sampling point is  $C_1 \setminus C_2 \dots C_n$ . Since the amount of air caused by air leakage is reduced, the SF6 concentration signal tends to be:  $C_1 < C_2 < \dots < C_n$ . Assume that the air volume at R1 is Q1, then the formula for calculating the air leakage in each section of the extension is as shown in formula (5.7):

$$\Delta Q_i = \frac{C_{i+1} - C_i}{C_{i+1} C_i} \times q$$

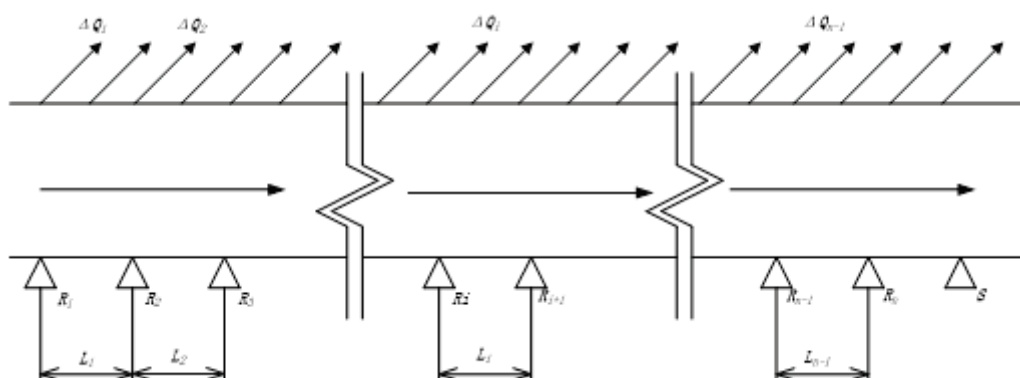


Figure 20 Diagram of Continuous Positive Pressure Air Leakage Measurement

The distance between the tracer gas release point and the sample point is calculated according to formula (5.8)

$$L \geq 32 \frac{S}{U}$$

L—Distance between tracer gas release point and sampling point, m;

S—Section area of working face, m<sup>2</sup>;

U—Workface perimeter length, m.

## 5.2.2 SF6 gas release and detection device

Sulfur hexafluoride is an odorless and colorless inert gas. The molecular mass is 146.07, the density is five times that of air, and the molecules are arranged on eight sides. The stability is extremely high, which is an excellent tracer gas for this experiment.

With the development of infrared technology, instruments using SF6 concentration measurement using infrared detection technology have been widely used in ground

working places, and the current SF6 infrared gas analyzer has less application in mine leakage detection, and no relevant manufacturers produce suitable The equipment is used by researchers and field staff.

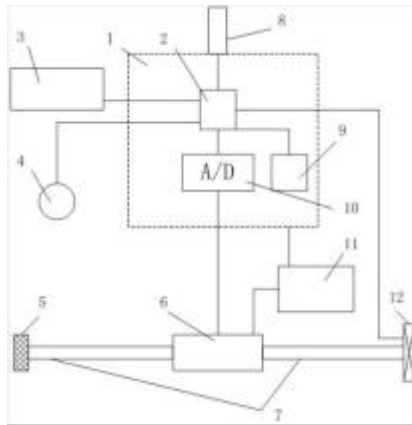
From the analysis of the instrument measurement principle, the measurement accuracy of the SF6 infrared gas analyzer is lower than that of the gas chromatograph (the accuracy of the infrared analyzer is ppm level, and the accuracy of the chromatograph is ppb level), but when the coal mine leaks, This accuracy is high enough to accurately measure air leakage, and the SF6 infrared gas analyzer has the advantage of real-time monitoring. If a memory card is installed on the SF6 infrared gas analyzer, automatic recording can be achieved. Therefore, when the SF6 infrared gas analyzer is used for air leakage measurement, the traditional air leakage measurement workload is greatly reduced, and the cycle is greatly shortened. This method is simpler and easier to implement than the conventional method, and at the same time, it is the concentration of SF6 at the monitoring site. The trend of change is completed, and the method can more accurately measure the amount of air leakage and obtain the law of change of air leakage.

#### (1) Instrument design

Figure 21 is a physical map of the portable mine SF6 tracer gas monitor designed and developed by the research group, and Figure 22 is a schematic diagram of the structure of the portable SF6 continuous analyzer. Two monitors were used in this project.



Figure 21 Physical map of sulphur hexafluoride



1 circuit board; 2 core controller; 3 human-computer interaction interface; 4 alarm indicator; 5 air inlet; 6 infrared gas sensor; 7 exhaust pipe; 8 RS232 interface; 9 memory card; 10 A/D converter; 11 power supply; 12 fans

**Figure 22 Schematic diagram of the structure**

### 5.2.3 Estimation of Tracer Gas Release

In order to detect the change of tracer gas concentration, it is necessary to estimate the amount of tracer gas released. This measurement uses sulfur hexafluoride as tracer gas. The portable sulfur hexafluoride detector has a range of 0-500 ppm, a resolution of 1 ppm and a sampling frequency of 3 seconds per time. Sulfur hexafluoride gas is released by continuous release method. Assuming that there is no air leakage to goaf, it is proposed to release 10 L/min, 50 L/min, 100 L/min and 200 L/min sulfur hexafluoride gas. The theoretical concentration detected is shown in Table 4.

**Table 4 Concentration values of different releases and corresponding theoretical measurements**

SF <sub>6</sub> Release rate (L/min)	Air volume (m <sup>3</sup> /min)	Theoretical detection concentration (ppm)
10	3000	3.33
50	3000	16.39
100	3000	32.25
200	3000	62.5

According to Table 5.3, when the release rate is 10 L/min, the theoretically detectable concentration is only 3.33 ppm in the 3000 m<sup>3</sup>/min wind flow. When the equipment detects a change of 1ppm, it is necessary to leak air into the goaf to be 1100m<sup>3</sup>/min,



which is obviously not realistic. Similarly, when the release rate is 50L/min, 100L/min, and 200L/min, when the 1ppm change is detected, the required air leakage amounts are: 220m<sup>3</sup>/min, 110m<sup>3</sup>/min and 55m<sup>3</sup>/min. According to theoretical calculations, when the release rate is 200 L/min, although more accurate results can be obtained, the release amount is too large, the proper release tool is not provided, and it is not economical. According to the literature and on-site wind loss estimation, the air leakage rate of Y-type ventilation is about 10%, that is, 300m<sup>3</sup>/min. When the release rate is 100L/min, the leakage of 110m<sup>3</sup>/min can theoretically be measured. Therefore, SF<sub>6</sub> should be taken. The release amount is controlled from 50 L/min to 100 L/min. At the same time, in order to ensure that a stable peak concentration can be captured, the release time is set to 1.5 min each time. Finally, the display in the flowmeter is 80L/min, because the measurement principle of this experiment is only based on the principle of gravity buoyancy balance, sulfur hexafluoride is an odorless and colorless inert gas. The molecular mass is 146.07, the density is five times that of air, and the molecules are arranged on eight sides. The stability is extremely high, which is an excellent tracer gas for this experiment. Since the molecular weight of sulfur hexafluoride is much larger than that of air, a large error is generated. Therefore, the device needs to be debugged before operation. After correction, the actual value of 80L/min displayed in the flowmeter is actually 57L/min.

---

#### **5.2.4 Measuring Point Arrangement Scheme**

---

The SF<sub>6</sub> release point and real-time monitoring point of W1310 working face are shown in Fig. 23.

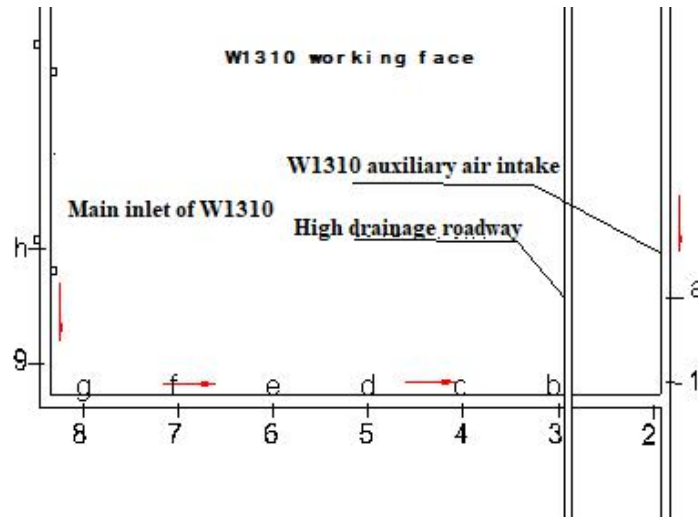


**Figure 23 Y Layout of Air Leakage Measuring Points in Working Face**

The numbers 1 to 9 are the positions of the SF6 monitoring points, and the letters a to h are the positions of the SF6 release points. The correspondence between the release points and the receiving points is shown in Table 5, and the spacing between the two adjacent points of the 2 to 8 monitoring points is 48m. In order to ensure that the release of SF6 sequence does not pollute the next set of measurements, therefore, "backward" release and measurement should be used, ie release and monitoring according to the sequence number of the SF6 release point, as shown in Table 5.

**Table 5 Corresponding relationship between SF6 monitoring points and release points**

Monitoring Point Number	Release Point Number
1	a
2	
3	b
4	c
5	d
6	e
7	f
8	g
9	h

The SF6 release point and real-time monitoring point of W1310 gob-side retaining roadway are shown in Fig. 24.

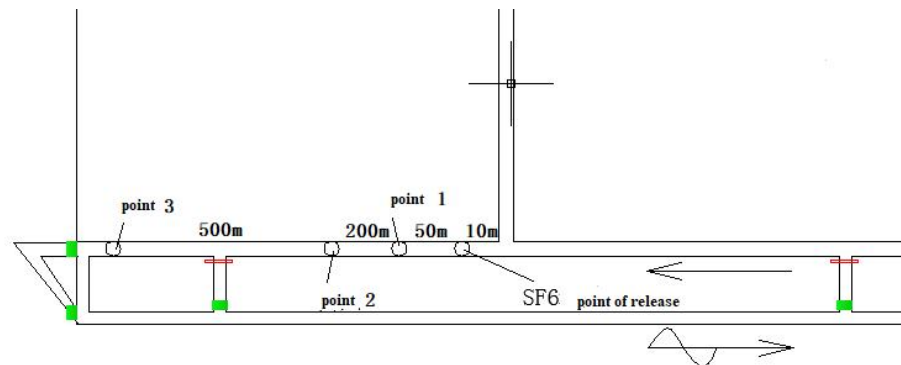


**Figure 24 Y Layout of Air Leakage Measuring Points in Gob side entry retaining**  
 Among them, the sulfur hexafluoride release point is 10 m away from the gob-side entry, and the 1, 2 and 3 measuring points are 50 m, 250m and 750 m away from the sulfur hexafluoride release point, respectively. After the release of sulfur hexafluoride from the release device, three groups of measuring points began to measure data at the same time.

### 5.2.5 data processing

After underground measurement, the data obtained from air leakage measurements of sulphur hexafluoride at different monitoring points in the working face are as follows.

**Table 6 Measured data of different monitoring points in working face**

point 2	point 3	point 4	point 5	point 6	point 7	point 8	point 9
0ppm	0ppm	0ppm	0ppm	0ppm	0ppm	1ppm	1ppm
1ppm	1ppm	0ppm	0ppm	1ppm	0ppm	1ppm	1ppm
2ppm	2ppm	1ppm	0ppm	2ppm	1ppm	1ppm	2ppm
4ppm	3ppm	2ppm	1ppm	2ppm	1ppm	2ppm	2ppm
6ppm	5ppm	5ppm	1ppm	4ppm	3ppm	3ppm	3ppm
7ppm	6ppm	6ppm	2ppm	4ppm	3ppm	4ppm	4ppm
8ppm	7ppm	7ppm	4ppm	5ppm	3ppm	5ppm	4ppm
8ppm	7ppm	8ppm	5ppm	5ppm	5ppm	6ppm	5ppm
9ppm	9ppm	9ppm	6ppm	6ppm	5ppm	8ppm	7ppm

12ppm	11ppm	12ppm	10ppm	7ppm	8ppm	8ppm	8ppm
12ppm	12ppm	13ppm	11ppm	8ppm	8ppm	10ppm	10ppm
14ppm	13ppm	13ppm	12ppm	9ppm	11ppm	11ppm	11ppm
15ppm	15ppm	14ppm	12ppm	11ppm	11ppm	11ppm	11ppm
16ppm	16ppm	15ppm	13ppm	12ppm	12ppm	12ppm	12ppm
18ppm	18ppm	17ppm	15ppm	13ppm	14ppm	13ppm	12ppm
18ppm	19ppm	17ppm	16ppm	14ppm	15ppm	13ppm	12ppm
20ppm	19ppm	18ppm	16ppm	15ppm	16ppm	14ppm	13ppm
23ppm	22ppm	22ppm	19ppm	17ppm	17ppm	17ppm	13ppm
24ppm	25ppm	22ppm	21ppm	18ppm	19ppm	17ppm	15ppm
25ppm	25ppm	24ppm	22ppm	21ppm	20ppm	18ppm	17ppm
25ppm	25ppm	23ppm	22ppm	21ppm	20ppm	18ppm	17ppm
25ppm	25ppm	24ppm	22ppm	21ppm	20ppm	19ppm	18ppm
22ppm	21ppm	22ppm	21ppm	20ppm	19ppm	19ppm	18ppm
19ppm	19ppm	20ppm	19ppm	18ppm	19ppm	18ppm	18ppm
18ppm	18ppm	17ppm	17ppm	16ppm	18ppm	18ppm	17ppm
17ppm	17ppm	16ppm	16ppm	15ppm	16ppm	19ppm	16ppm
16ppm	17ppm	15ppm	13ppm	14ppm	13ppm	17ppm	15ppm
15ppm	15ppm	14ppm	12ppm	12ppm	11ppm	15ppm	14ppm
14ppm	13ppm	12ppm	11ppm	11ppm	10ppm	11ppm	13ppm
13ppm	13ppm	12ppm	11ppm	11ppm	10ppm	10ppm	12ppm
12ppm	10ppm	11ppm	9ppm	9ppm	9ppm	10ppm	11ppm
10ppm	9ppm	8ppm	8ppm	8ppm	7ppm	9ppm	10ppm
9ppm	7ppm	8ppm	6ppm	6ppm	6ppm	8ppm	8ppm
7ppm	7ppm	6ppm	6ppm	5ppm	4ppm	7ppm	7ppm

7ppm	7ppm	6ppm	5ppm	5ppm	5ppm	6ppm	6ppm
5ppm	6ppm	4ppm	4ppm	4ppm	4ppm	5ppm	5ppm
3ppm	3ppm	3ppm	3ppm	3ppm	3ppm	4ppm	5ppm
2ppm	2ppm	2ppm	1ppm	3ppm	2ppm	3ppm	5ppm
1ppm	1ppm	1ppm	1ppm	3ppm	1ppm	4ppm	4ppm
1ppm	1ppm	1ppm	1ppm	2ppm	1ppm	3ppm	4ppm
0ppm	0ppm	0ppm	0ppm	1ppm	1ppm	2ppm	3ppm
0ppm	0ppm	0ppm	0ppm	1ppm	1ppm	2ppm	4ppm
0ppm	0ppm	0ppm	0ppm	2ppm	1ppm	2ppm	2ppm
0ppm	0ppm	0ppm	0ppm	1ppm	1ppm	2ppm	2ppm
0ppm	0ppm	0ppm	0ppm	1ppm	1ppm	2ppm	3ppm
0ppm	0ppm	0ppm	0ppm	1ppm	0ppm	2ppm	2ppm
0ppm	0ppm	0ppm	0ppm	1ppm	0ppm	2ppm	2ppm
0ppm	0ppm	0ppm	0ppm	0ppm	0ppm	1ppm	1ppm
0ppm	0ppm	0ppm	0ppm	0ppm	0ppm	1ppm	0ppm

According to the average value of the measured data from 9 monitoring points, the concentration distribution of sulfur hexafluoride at each monitoring point can be obtained as shown in Fig. 25 and Fig. 26.

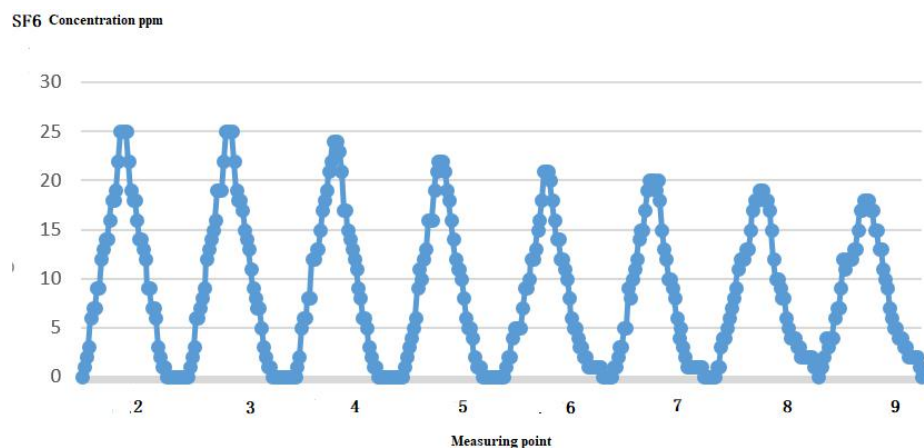


**Figure 25 Continuous monitoring data of sulphur hexafluoride at 9 measuring points in working face**

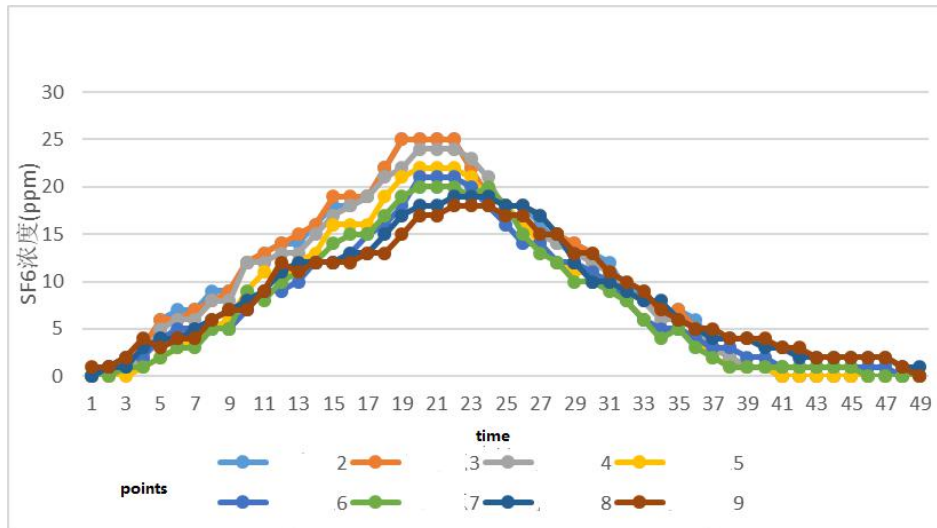


**Figure 26 Monitoring data of sulphur hexafluoride at each measuring point in working face**  
 The data obtained from the air leakage measurement of sulfur hexafluoride at different monitoring points along goaf retaining roadway are as follows: Table 7

**Table 7 Sulfur hexafluoride concentration data for gob-side entry retaining**

Point1	Point2	Point3
0ppm	0ppm	0ppm
0ppm	0ppm	1ppm
0ppm	1ppm	2ppm
1ppm	1ppm	3ppm
3ppm	2ppm	6ppm
5ppm	5ppm	8ppm
5ppm	6ppm	9ppm
7ppm	7ppm	10ppm
8ppm	9ppm	11ppm
9ppm	9ppm	12ppm
10ppm	10ppm	14ppm
12ppm	12ppm	16ppm
13ppm	14ppm	17ppm
13ppm	13ppm	18ppm
14ppm	14ppm	20ppm
14ppm	13ppm	22ppm

16ppm	16ppm	23ppm
17ppm	18ppm	23ppm
18ppm	19ppm	23ppm
19ppm	19ppm	23ppm
19ppm	19ppm	22ppm
16ppm	17ppm	20ppm
15ppm	14ppm	17ppm
12ppm	12ppm	11ppm
9ppm	8ppm	11ppm
5ppm	5ppm	8ppm
2ppm	3ppm	7ppm
1ppm	2ppm	6ppm
0ppm	1ppm	3ppm
0ppm	0ppm	2ppm
0ppm	0ppm	1ppm

By calculating the average value of the field measured data from each monitoring point, the concentration distribution of sulfur hexafluoride at five monitoring points can be obtained as shown in Fig. 27 and Fig. 28.

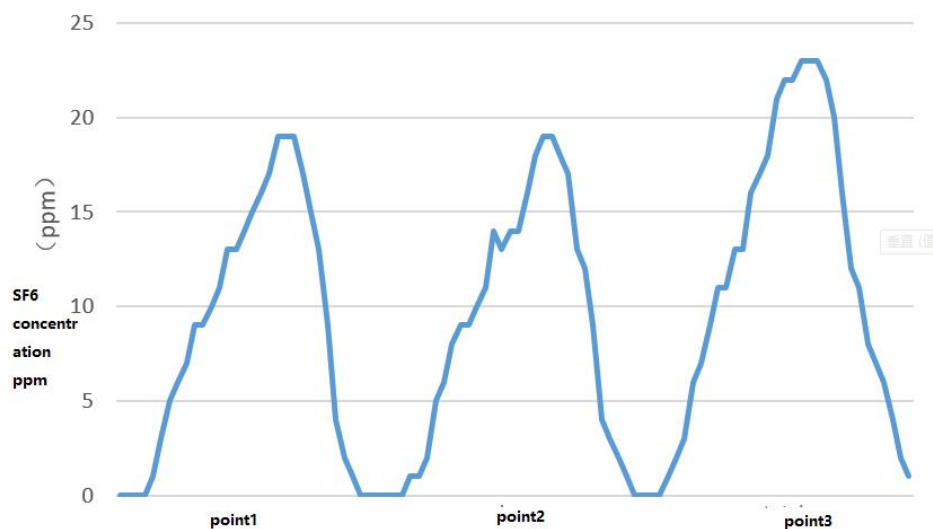


**Figure 27 Continuous monitoring data of sulfur hexafluoride at three measuring points along goaf retaining roadway**

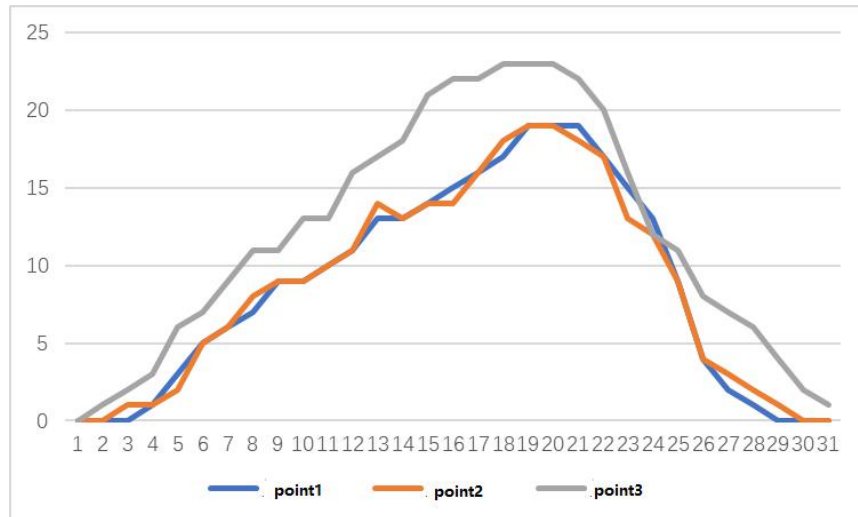


**Figure 28 Monitoring data of sulphur hexafluoride at each measuring point of gob-side entry retaining**

It can be seen from the graph that the peak value of sulfur hexafluoride monitoring for three times is 19 ppm, 19 ppm and 23 ppm. The monitoring points are separated by 30 m. There is almost no air leakage in the working face of gob-side entry. There is more air leakage in the working face of gob-side entry, less air leakage near the working face and more air leakage in the position far from the working face.

### 5.2.6 Result and Analysis

According to the measured data of air tester and the calculation of sulfur hexafluoride concentration, the receiving peak values of sulfur hexafluoride in nine working faces are stable at 77 ppm, 25 ppm, 25 ppm, 24 ppm, 22 ppm, 21 ppm, 20 ppm, 19 ppm and 18 ppm. The corresponding air volume at each monitoring point is as follows: Table 8.

**Table 8 Air volume of monitoring points in working face**

Point	1	2	3	4	5	6	7	8	9
Air volume ( $\text{m}^3/\text{min}$ )	736	2302	2302	2382	2537	2657	2817	2967	3200

**Table 9 Air leakage between monitoring points in working face**

Point	1	2	3	4	5	6	7	8	9
air leakage rat ( $\text{m}^3/\text{min}$ )	0	0	80	155	120	160	150	233	0

The difference of SF6 concentration is converted into the variation of air volume between two adjacent measuring points by sorting out and analyzing the measured data of air leakage. Fig. 29 is shown.



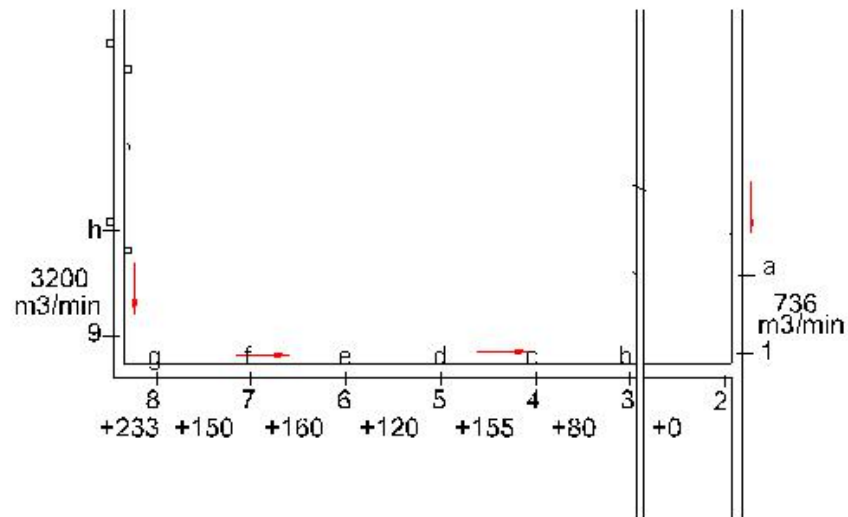


**Figure 29 Y Air Leakage Distribution in Working Face**

The “+” in Figure 29 represents the air leakage in the working area. Through the actual measurement of the air leakage of the Y-type working face of Gaohe Coal Mine, it can be seen that the total air leakage of the working face into the goaf is 898 m<sup>3</sup> / min. The working surface tape has more air leakage in the direction of the air inlet of the slot in the range of 60 m. The wind entering the goaf is 233 m<sup>3</sup>/min; the direction of the cut-in airflow is in the range of 0m~250m, due to the structure of the Y-type ventilation system and the extraction of the high-drainage roadway (the extraction volume of the high-drainage roadway is about It is 400m<sup>3</sup>/min), causing it to leak into the goaf and the air leakage is large.

(2) Analysis of air leakage data along the empty roadway:

The peaks of sulphur hexafluoride reception at three monitoring points along the empty roadway are stable at 19ppm, 19ppm and 23ppm. According to the measured wind volume and the concentration of sulphur hexafluoride, the corresponding air volume of each monitoring point is shown in Table 10 below.

**Table 10 Air volume of monitoring points in gob-side entry retaining**

Point	1	2	3
Air volume (m <sup>3</sup> /min)	2630	2630	2100

**Table 11 leakage between monitoring points in gob-side entry retaining**

Air leakage interval	0-1	1-2	2-3
air leakage rat (m <sup>3</sup> /min)	0	0	500

In order to find the air leakage range of the Y-shaped working face along the roadway in Gaohe Coal Mine, the air volume change along the empty roadway was tested by

releasing SF6 on the empty roadway. The final measurement found that the Y-shaped working face had no gobs leaking into the air within 260 meters in front of the empty roadway. The air leakage is mainly concentrated in the range of 260 meters to 760 meters, and the air leakage in this section is about 500 cubic meters per minute [58] as shown in Figure 30.

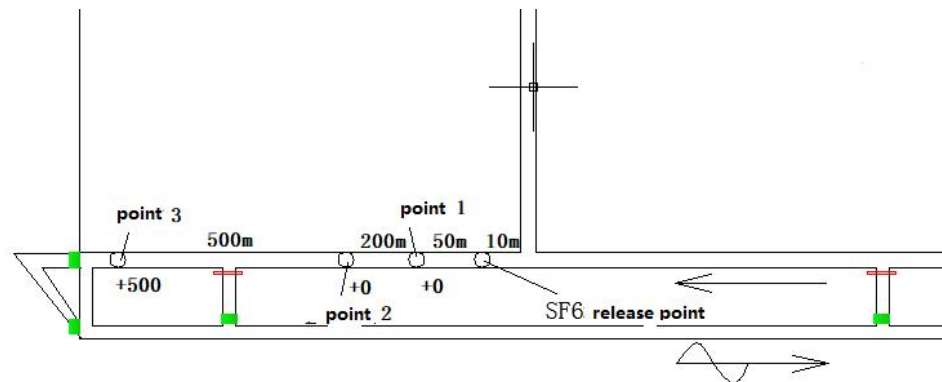


Figure 30 Y Leakage Distribution of Gob-side Retaining Roadway in Working Face

### 5.3 Summary of this chapter

In this chapter, field measurements were carried out on W1310 working face in Gaohe Coal Mine. According to the previous simulation results, the pressure energy at different depths of working face was measured correspondingly, and the variation law of pressure energy in the direction of working face was summarized. The dynamic simulation map of three-dimensional ventilation in mine was established. By using SF6 tracer gas leak detector, the pressure energy was measured through instrument optimization and reasonable distribution of measuring points. The air leakage at different depths in the direction of the working face is calculated, which corresponds to the simulation results and verifies the validity of the simulation results. In the future, the simulation results of gas distribution and air flow curve in goaf can provide guidance for preventing spontaneous combustion in goaf and optimizing gas extraction scheme design.

---

## 6 Conclusion

---

### 6.1 Main conclusions

---

(1) The mechanical properties of overlying strata in goaf of Y-type working face in Gaohe Coal Mine are studied theoretically. Through the application of UDEC numerical simulation software. The roof caving situation of the goaf in W1310 working face is obtained. The calculation shows that the height of the caving zone in Y-type working face is 30m and the height of the fissure zone is 35m. Then, according to the relationship between void and permeability in goaf and the theory of "O" circle, the permeability model of W 1310 in this Y-shaped working face is established.

(2) The flow field distribution in goaf was simulated by COMSOL software, and the concentration distribution of gas in goaf under different conditions was found out. Under the action of high extraction roadway, the air flow trajectory inside the goaf has changed greatly due to the drainage effect of high extraction roadway. A large amount of air flow in the goaf is withdrawn from the high extraction roadway, only the latter part of the air flow in the flexible membrane wall leaks back to the goaf retaining roadway.

(3) By measuring the resistance of mining area, a three-dimensional ventilation network calculation model of mine is established based on Ventsim software, which provides a reference for the analysis of air leakage caused by the pressure difference of working face and the change of relative pressure along goaf retaining Lane under different adjustments. The pressure and energy changes of Y-type working face and goaf retaining Lane in Gaohe Coal Mine are measured in detail, and the leakage of working face is analyzed based on pressure and energy. The results show that the air volume decreases gradually from the lower corner of the cut hole to 180 m, and the air pressure is basically stable from 180 m to 305 M.

According to the SF6 air leakage measurement of Y-type working face in Gaohe Coal Mine, the total air leakage to goaf is 898 m<sup>3</sup>/min, and the air leakage is more in the front 60 m of the direction of the belt inlet along the trough, 233 m<sup>3</sup>/min air leakage to goaf, and 0 m~250 m of the direction of the air leakage to the cutting hole. The simulation results are validated. In the future, the simulation results of gas distribution and air flow curve in goaf can provide guidance for the design of goaf natural fire prevention and gas optimal extraction scheme.

---

## 6.2 Outlook

---

(1) This paper only simulates the gas flow field in the Y-type ventilation goaf of two-way and one-way working face. Therefore, the simulation results of goaf gas field will certainly have some shortcomings, and further research is needed in the future.

(2) The simulation focuses on the influence of air distribution on the gas migration in goaf. There is not much research on the influence of extraction and rock pressure on the gas migration in goaf. More careful research should be done in the future.

(3) The application of this paper in practical work still needs to be discussed. In the future, it can be considered to play a guiding role in gas control in goaf.

---

## 6.3 Innovation points

---

(1) Development of a sulphur hexafluoride determination and analysis system for coal mines. The system includes a portable SF<sub>6</sub> analyzer and SF<sub>6</sub> data processing and analysis software. The portable SF<sub>6</sub> analyzer realizes large-scale, long-term SF<sub>6</sub> concentration automatic monitoring and storage, and SF<sub>6</sub> data processing and analysis software. The SF<sub>6</sub> optimal release estimation, common rotor flowmeter scale conversion, SF<sub>6</sub> monitoring value tracking display and air leakage automatic calculation are realized. The system can realize quantitative detection of mine air leakage passage and air leakage.

(2) Based on the sulphur hexafluoride determination and analysis system for coal mines, the air leakage path and air leakage volume of the coal mine working in the goaf and the goaf through the soft film wall to the roadway are determined quantitatively.

---

## 7 Bibliography

---

### references

- [1] Li Shengzhou. Study on the evolution of overburden fracture field and gas migration law [D]. Chongqing University, 2012.
- [2] Hou Songfeng. Comparative Study on Air Flow and Gas Migration in Two Ventilation Modes[J]. Energy Technology and Management, 2014,39(04):38-40.
- [3] Wu Gang, Dong Jiamei, Zhao Jianhua. Research on Gas Control Technology in Coal Face[J]. Coal Technology, 2008(06): 99-100.
- [4] Fan Hongwei. Numerical simulation study on gas migration law in goaf of fully mechanized caving face[D]. Taiyuan University of Technology, 2010.
- [5] Zhang Wei. Gas seepage law and numerical simulation of goaf in fully mechanized caving face [D]. Xi'an University of Science and Technology, 2008.
- [6] Han Guang. Research on Distribution Law and Treatment of Y-type Ventilation Gas[J]. Private Science and Technology, 2014(10): 19.
- [7] Zheng Jiyu, Han Chunlei, Xu Hui, et al. Study on gas source and distribution law of fully mechanized caving face[J]. Coal Technology, 2015,34(03):126-129.
- [8] Han Jianwei. Application Analysis of Gas Control Technology in Fully Mechanized Face of High Gas Mine[J]. Shandong Coal Science and Technology, 2016(05): 64-65.
- [9] Suo Liang. Gas migration law of Y-type ventilation working face along the roadway and its application [D]. Xi'an University of Science and Technology, 2014.
- [10] Zhu Xiaodong. Research on gas migration law of Y-type ventilation goaf without coal pillar [D]. Anhui University of Science and Technology, 2011.
- [11] Hu Qianting, Liang Yunpei, Liu Jianzhong. CFD simulation of gas flow law in goaf[J]. Journal of China Coal Society, 2007(07): 719-723.
- [12] Liu Jun, Zhao Yajun, Zhang Xiaojun. Analysis of Gas Drainage Technology in Fully Mechanized Face of Coal Mine[J]. Inner Mongolia Coal Economy, 2016(22): 136-137.
- [13] Zhou Jiachuan. Research and application of gas drainage technology in goaf [D]. Taiyuan University of Technology, 2012.
- [14] Yang Da, Zhou Dan. Determination of Gas Source Measurement in Coal Face[J]. Shenhua Science and Technology, 2015,13(04):33-34.
- [15] Yang Xiujun. Study on the distribution law of gas concentration in goaf[J]. Science and Technology Information, 2013(23): 98-100.
- [16] Zhang Yanbin, Qin Zikai, Yu Xinhe, et al. Study on Gas Migration Law of Fully Mechanized Caving Face in High Gassy Coal Seam[J]. Coal Mining, 2015, 20(02): 81-84.
- [17] Wang Xu, Hao Yingge, Song Xianming, et al. Research and practice of air leakage control technology in large area goaf in Nantun Coal Mine, 2011[C].
- [18] Huang Bingxiang, Liu Changyou, Cheng Qingying, et al. Simulation test of roof caving law based on gas drainage[J]. Chinese Journal of Rock Mechanics and Engineering, 2006(11): 2200-2207.

- [19] YUAN Liang. Theory and Practice of Co-production of Coal-free Column Gas in Low Permeability Coal Seam Group[J]. China Engineering Science, 2009,11(05):72-80.
- [20] Zhu Aijun. Stability of nanofluids and their convective heat transfer characteristics [D]. Jiangsu University, 2010.
- [21] Zhu Lin, Xu Jinliang, Kong Fanrang, et al. Effect of hydrogen/air equivalence ratio on combustion characteristics of micro-combustor[J]. Editorial Office of Optics and Precision Engineering, 2008(11): 2214-2221.
- [22] Cui Yiyuan. Study on air leakage in goaf based on tracer gas measurement technology [D]. China University of Mining and Technology (Beijing), 2018.
- [23] Guo Lei. Numerical simulation of ventilation in long-distance single-head tunnel construction [D]. Lanzhou Jiaotong University, 2010.
- [24] Dai Zhongyuan. Numerical simulation of the performance of a certain type of plate-fin heat exchanger based on FLUENT and its structural optimization [D]. Wuhan University of Technology, 2013.
- [25] Wang Honggang. Research on superposition method of airflow field and gas migration in goaf [D]. Xi'an University of Science and Technology, 2009.
- [26] Yu Lianli. Numerical simulation and experimental study of gas-solid two-phase flow in pulverized coal drying pipe [D]. Liaoning University of Engineering and Technology, 2009.
- [27] Chen Shanle. Study on seepage field and permeability coefficient of goaf in fully mechanized caving face[D]. Liaoning University of Engineering and Technology, 2015.
- [28] Guo Shan. The height of the “three belts” in the 8206 working face of Mabao Coal Mine is determined [J]. Tongmei Technology, 2016(06): 17-22.
- [29] Shi Weigang. Research on the theoretical basis of waterproof and isolated coal pillars in adjacent and isolated working faces [D]. Xi'an University of Science and Technology, 2015.
- [30] Ren Zhuochen. Study on the coupling of explosion and explosion in goaf in high gassy and spontaneous combustion coal seam [D]. Xi'an University of Science and Technology, 2017.
- [31] Xia Xiaogang. Research on “Four Belts” Model of Mining Rock Stratum and Surface Movement [D]. Xi'an University of Science and Technology, 2012.
- [32] Song Yang. Numerical simulation of deformation and failure of overlying strata in shallow coal seams[J]. Heilongjiang Science and Technology Information, 2015(18): 24-26.
- [33] Sun Chen, Feng Kangwu, Qi Jun, et al. Numerical study on gas seepage characteristics of protective layer mining based on stress-seepage coupling[J]. Inner Mongolia Coal Economy, 2016(15):139-145.
- [34] Mei Zhenhua. Research on gas migration and heat storage area determination in goaf [D]. Xi'an University of Science and Technology, 2010.
- [35] Li Zhifeng, Liu Jiajia, Wang Dan. Simulation Study on Gas Distribution Law in Goaf[J]. Coal, 2012, 21(10): 1-3.
- [36] Li Zongxiang. The Theory of Field Flow Safety in Goaf and Its New Progress[J]. China Safety Science Journal, 2005(12): 85-88.

- [37] Chen Hema, Ren Hongan. Numerical Simulation of Gas Flow Field in Goaf under Different Conditions[J]. Shaanxi Coal, 2013,32(03): 7-9.
- [38] Chen Peng, Zhang Lang, Zou Dongqi. Study on Three-Dimensional Permeability Distribution of Goaf Based on "O" Ring Theory[J]. Mining Safety and Environmental Protection, 2015,42(05):38-41.
- [39] Li Gang, Liang Bing. Formation mechanism and application of seepage field in overburden strata: The 9th National Symposium on Seepage Mechanics, Xi'an, Shaanxi, China [C].
- [40] Hu Dongxiang. Preliminary study on the mechanism of water inrush from the overburden strata in Jining coalfield[J]. Energy Technology and Management, 2010(01): 94-96.
- [41] Lu Qian. Research on relationship between mining fissure and gas distribution in coal seam roof[J]. China Coal, 2009,35(12):89-91.
- [42] Guo Houyang. Study on distribution and prevention and control technology of coal spontaneous combustion in goaf of Y-type ventilated working face in high gassy and spontaneous combustion coal seam[D]. Anhui Jianzhu University, 2014.
- [43] Cai Jinlong. Research on overburden failure and load transfer law in extra-thick coal seam mining[D]. Anhui University of Science and Technology, 2013.
- [44] Liu Mingxin. Research on Gas Drainage Technology in High-drainage Roadway of 9101 Working Face in Wangzhuang Coal Mine[D]. Henan Polytechnic University, 2015.
- [45] Liu Jiajia. Study on flow field and gas distribution law in goaf of fully mechanized mining face[D]. Henan Polytechnic University, 2011.
- [46] Li Xia. Study on the law of gas migration in ventilation system of "one enter and two return" working face [D]. Taiyuan University of Technology, 2010.
- [47] Jin Lingzi. Research on gas migration law in goaf of fully mechanized caving face in Tashan Coal Mine [D]. Liaoning University of Engineering and Technology, 2012.
- [48] Tao Zhanyu. Numerical Simulation of the Influence of Air Leakage on the Gas Migration Law in Goaf[J]. Coal Engineering, 2014, 46(11): 102-105.
- [49] Cao Wenchao, Liu Jun, Chen Xueming. Simulation of Gas Drainage in the Gob of Mining Face[J]. Coal Technology, 2016,35(07):206-208.
- [50] Xu Wei, Yan Liangfeng. Numerical Simulation of Gas Flow Field in Y-type Ventilation Goaf[J]. Journal of Anhui University of Science and Technology (Natural Science), 2010, 30(03): 29-31.
- [51] Sun Dongsheng. Research and application of gas control technology in goaf of 1011 fully mechanized mining face in Yuandian No.1 Mine [D]. Anhui University of Science and Technology, 2014.
- [52] Chen Jianqiang, Wei Yinshang. Stability Analysis of Ventilation System in Jiaogou Coal Mine[J]. Journal of Xi'an University of Science and Technology, 2010,30(05):531-535.
- [53] Zhang Shuchuan. Method for Measuring Resistance of Mine Ventilation System and Error Analysis[J]. Mining Safety and Environmental Protection, 2014,41(02):93-96.
- [54] Zhang Yingxin. Analysis of Resistance Measurement of Mine Ventilation Network[J]. Modernization of Coal Mines, 2009(02): 49-50.

- [55] Deng Lijun. Inversion of mine ventilation resistance coefficient [D]. Liaoning University of Engineering and Technology, 2014.
- [56] Qu Fang, Liu Kegong, Li Yingye, et al. Error Analysis of Mine Ventilation Resistance by Barometer Method and Selection of Base Point Location[J]. Coal Mine Safety, 2004(06): 10-12.
- [57] Zhang Chao. Research on coal spontaneous combustion detection and prediction technology in lower layer working face [D]. Anhui University of Science and Technology, 2017.
- [58] Xue Junhua. Y-type ventilation coal and gas co-production technology in three lanes[J]. Journal of Anhui Institute of Architecture & Industry, 2012, 20(04): 83-90.



---

## 8 List of Figures

---

Figure 1 Empirical Model Permeability Distribution.....	16
Figure 2 Empirical Model Permeability Distribution.....	17
Figure 3 Empirical Model Permeability Distribution.....	18
Figure 4 Theoretic schematic diagram of O-ring.....	18
Figure 5 UDEC simulation results.....	22
Figure 6 Vacancy distribution in Goaf.....	22
Figure 7 Permeability Model of Caving Zone in Goaf.....	23
Figure 8 Y Working Face Model.....	25
Figure 9 Wind Trajectory.....	26
Figure 10 Overall Gas Distribution in Goaf.....	27
Figure 11 z = 1.5 m gas distribution.....	27
Figure 12 z = 10m gas distribution.....	28
Figure 13 z = 32m plane gas distribution.....	28
Figure 14 Gas Profile of Goaf.....	29
Figure 15 Gas Control Model of High Drainage Roadway.....	29
Figure 16 Air flow trajectory in goaf under high pumping condition.....	30
Figure 17 Gas distribution in Goaf.....	30
Figure 18 Relative Pressure Distribution Diagram of Air Flow in Working Face.....	36
Figure 19 Retaining Roadway along Gob.....	36
Figure 20 Diagram of Continuous Positive Pressure Air Leakage Measurement.....	38
Figure 21 Physical map of sulphur hexafluoride.....	39
Figure 22 Schematic diagram of the structure.....	40
Figure 23 Y Layout of Air Leakage Measuring Points in Working Face.....	42
Figure 24 Y Layout of Air Leakage Measuring Points in Gob side entry retaining.....	43

Figure 25 Continuous monitoring data of sulphur hexafluoride at 9 measuring points in working face.....	45
Figure 26 Monitoring data of sulphur hexafluoride at each measuring point in working face.....	46
Figure 27 Continuous monitoring data of sulfur hexafluoride at three measuring points along goaf retaining roadway.....	47
Figure 28 Monitoring data of sulphur hexafluoride at each measuring point of gob-side entry retaining.....	48
Figure 29 Y Air Leakage Distribution in Working Face.....	49
Figure 30 Y Leakage Distribution of Gob-side Retaining Roadway in Working Face.	50

---

## 9 List of Tables

---

Table 1 Flow field and gas concentration distribution in goaf under different ventilation modes.....	1
Table 2 Table of mechanical parameters of UDEC simulated strata.....	20
Table 3 Distribution Table of Relative Pressure of Air Flow in Working Face.....	36
Table 4 Concentration values of different releases and corresponding theoretical measurements.....	40
Table 5 Corresponding relationship between SF6 monitoring points and release points .....	42
Table 6 Measured data of different monitoring points in working face.....	43
Table 7 Sulfur hexafluoride concentration data for gob-side entry retaining.....	46
Table 8 Air volume of monitoring points in working face.....	48
Table 9 Air leakage between monitoring points in working face.....	48
Table 10 Air volume of monitoring points in gob-side entry retaining.....	49
Table 11 leakage between monitoring points in gob-side entry retaining.....	49

## Thesis Grade

**Thesis:** Study on the influence of air leakage in working face on gas flow field  
in goaf of Y-type ventilation system

**Author:** Haohui Shi

**Supervisor:** Bing Wu **Grade:** 88 **Signature:** Bing Wu.

**Co-Supervisor:** \_\_\_\_\_ **Grade:** \_\_\_\_\_ **Signature:** \_\_\_\_\_